Merging Multi-OMICs with Proteome Integral Solubility Alteration Unveils Antibiotic Mode of Action

Ritwik Maity[123], Xuepei Zhang[7,8,9], Francesca Romana Liberati[6], Francesca Cutruzzolà[6], Serena Rinaldo[6], Massimiliano Gaetani[7,8,9], José Antonio Aínsa[1345], Javier Sancho[123#]

[1] Biocomputation and Complex Systems Physics Institute (BIFI)-Joint Units: BIFI-IQFR (CSIC) and GBsC-CSIC, University of Zaragoza, 50018 Zaragoza, Spain

[2] Departamento de Bioquímica y Biología Molecular y Celular, Faculty of Science, University of Zaragoza, 50009 Zaragoza, Spain

[3] Aragon Health Research Institute (IIS Aragón), 50009 Zaragoza, Spain

[4] Departamento de Microbiología, Pediatría, Radiología y Salud Pública, Faculty of Medicine, University of Zaragoza, 50009 Zaragoza, Spain

[5]CIBER de Enfermedades Respiratorias—CIBERES, Instituto de Salud Carlos III, 28029 Madrid, Spain

[6] Department of Biochemical Sciences "A. Rossi Fanelli", Sapienza University of Rome, 00185 Rome, Italy

[7] Department of Medical Biochemistry and Biophysics, Karolinska Institutet, Stockholm, Sweden

[8] Chemical Proteomics Unit, Science for Life Laboratory (SciLifeLab), Stockholm, Sweden

[9] Chemical Proteomics, Swedish National Infrastructure for Biological Mass Spectrometry (BioMS), Stockholm, Sweden

[#]Correspondence to J. Sancho (jsancho@unizar.es)

Abstract

Antimicrobial resistance is responsible for an alarming number of deaths, estimated at 5 million per year. To combat priority pathogens, like *Helicobacter pylori,* the development of novel therapies is of utmost importance. Understanding the molecular alterations induced by medications is critical for the design of multi-targeting treatments capable of eradicating the infection and mitigating its pathogenicity. However, the application of bulk omics approaches for unravelling drug molecular mechanisms of action is limited by their inability to discriminate between target-specific modifications and off-target effects. This study introduces a multi-omics method to overcome the existing limitation. For the first time, the PISA assay is utilized in bacteria in the PISA-express format to link proteome solubility with different and potentially immediate responses to drug treatment, enabling us the resolution to understand target-specific modifications and off-target effects. This study introduces a comprehensive method for understanding drug mechanisms and optimizing the development of multi-targeting antimicrobial therapies.

Introduction

Antimicrobial resistance (AMR) poses a global threat of profound proportions. It is estimated that drug-resistant infections contribute to nearly 5 million deaths every year[1]. The development of new, ideally narrow-spectrum antibiotics for "Priority pathogens" is one of the key factors in reducing the toll, along with international cooperation, vaccines and diagnostics. *Helicobacter pylori (H. pylori)* is one of the high-priority pathogens[2] in the World Health Organization (WHO) list of bacteria for which new antibiotics are urgently needed. A meta-study published in 2018 has estimated *H. pylori* infection has a prevalence of 44.3% worldwide[3]. The eradication of *H. pylori* is carried out using either triple or quadruple chemotherapy, in which several antibiotics and antimicrobial compounds including bismuth are used in combination with a proton pump inhibitor (PPI). A recent meta-analysis from published US studies estimated the individual rate of resistance for clarithromycin, metronidazole, and levofloxacin to be higher than 30%.[4] This urges the development of new, ideally narrow-spectrum, antibiotics for the treatment of drug-resistant *H. pylori*. Essential metabolic pathways are a vast promising scenario for antimicrobial development. Flavodoxin, urease, menaquinone synthesis enzymes and respiratory complexes are among the most promising potential disease-specific targets for obtaining narrow-spectrum anti-*H. pylori* agents[5–7]. In this study, we have used five compounds developed from a high-throughput screening conducted to identify inhibitors against *H. pylori* flavodoxin (Hp-Fld)[8]. Hp-Fld is an essential protein for *H. pylori,* and it is not present in humans as an independent protein, which makes it a preferred candidate for anti-*H. pylori* drug development. The selected compounds (Fig S1(A)) derive from 4-nitrobenzoxadiazole (IV and IV-j) or 4-amine benzoxadiazole (IVa and IVk) and differ in terms of solubility and antimicrobial specificity spectrum. IVb is a hydrophobic analogue not having a benzoxadiazole moiety.

The identification of the modes of action of new potential drugs is a major challenge in the chemical systems biology of diseases and there are numerous bioactive compounds (including approved drugs) whose mechanisms of action remain unknown[9,10]. Whether identifying the mode of action of a new antibiotic is a medical priority can be debated. However, a mechanistic understanding at the molecular level is of immense benefit to its future development as a drug. The mode of action of an antibiotic is generally classified depending on the interaction with its target, which is often a protein essential for maintaining bacterial viability. However, as with any drug, an antibiotic may interact not only with its primary target but also with other unexpected targets in the bacterium or the host (off-targets)[11]. This may cause

unforeseen side effects that, although typically undesired, may occasionally enable new therapeutic indications.

Target-based drug discovery pipelines rely on *in vitro* screening protocols mostly monitoring drug-target (usually a protein) binding or concomitant changes in protein stability. Despite their scalability and adaptivity, these protocols may or may not accurately represent the drug's target and off-target interactions *in vivo*. Recent developments in omics techniques can provide a molecular-level view of drug-induced changes in cellular processes. The robustness of omics techniques in pathway prediction has been demonstrated and a wide range of life science fields increasingly rely on them. Compared to conventional approaches, omics techniques provide a more holistic molecular perspective on biological systems. While large-scale omics data are becoming more accessible, and multi-omics studies are more frequent, multi-omics integration of data remains challenging. Here we propose a post-analysis data integration method for pathway prediction and validation of the mechanism of action of Hp-Fld inhibitors. It is a long-standing knowledge that, when heated, proteins denature and generally become insoluble, and interaction with small molecules can induce changes in the thermal stability and solubility of proteins. Thermal shift assay (TSA)[12] utilizes this knowledge to understand drug-protein interaction by observing the target's melting temperature shift upon drug treatment. However, when the target is uncertain or the mechanism is to be elucidated, the use of omics techniques must consider different angles to be able to deconvolute changes in the system as a whole upon drug treatment. The deconvolution of unknown targets using TSA-based proteomics approaches[12] shows some technical biases and a limited throughput to be able to compare multiple drugs in a significant number of biological replicates and to be able to integrate other omics approaches. To address those issues, we adopt here an approach based on the unbiased and high-throughput target deconvolution method known as the Proteome Integral Solubility Alteration (PISA) assay in the PISA-express format[13–16]. It is based on the fact that protein targets, as well as other early mechanistic proteins, may undergo changes in solubility as a result of drug binding or changes in related molecular interactions and macro complexes within a cell. The information obtained on the protein targets of the individual compounds has been utilized to filter the differential expression data from proteomics and transcriptomics, aiming to identify the most influenced pathways. Subsequently, we validated selected pathways at a functional level.

Results

Changes in transcriptomics and proteomics landscape, and associated gene ontology

Our investigation into understanding the mode of action of nitro-benzoxadiazole compounds commenced with a comparison of the transcriptional and translational changes induced by these compounds, the vehicle control (DMSO), and the commercially used drug metronidazole. RNA sequencing (RNA-seq) and expressional proteomics were employed to identify transcriptional and translational changes, respectively. A total of 771 differentially expressed transcripts (Fig S1(D)) and 113 (Fig S1(E)) differentially expressed proteins were selected using a linear model fitting analysis followed by a cutoff-based selection. Overall, we have achieved more then 90% of genomic coverage and more than 25% of the transcripts and 10% of the proteins were found to be differentially expressed upon treatment except for compound IVk, which exhibited 372 differentially expressed proteins in spite of the fact that only 11 transcripts showed differential expression at a p-value of 0.001 and 175 at a p-value of 0.05. The differentially expressed transcripts in the presence of the individual drugs were investigated using gene set enrichment analysis (GSEA) (Fig. S2(A-G)).

We compared transcriptomics and proteomics data for the lead compound IV (Fig. 1(A)) and found 174 common IDs (gene or protein). These IDs shows enrichment in gene ontology terms "Protein containing complex", "Cellular anatomical entity", "Proton-transporting ATP synthase complex" and "Non-membrane-bounded organelle". Two GO terms, "Metabolic process (GO:0008152)" and "Organonitrogen compound biosynthetic process (GO:1901566)", are present in all compounds except for compound IVk (Fig. 1(E)). Some analogies for pairs of compounds sharing either the nitro, the amine group or the polar moiety stand out. For example, the "Proton-transporting ATP synthase complex (GO:0045259)" is found in the nitro-containing compound IV (Fig. 1(A)), while its soluble derivative, compound IVj, is the only compound containing the "ATP metabolic process (GO:0046034)" and "ATP synthesis coupled proton transport (GO:0015986)" (Fig. 1(D)), suggesting IVj exerts a specific effect on ATP production and utilization. ATP synthase-related functions are thus relevant in the two closely related nitro compounds tested. On the other hand, both compound IVa (Fig. 1(B)) and its soluble derivative IVk (Fig. 1(E)) share the ontology term related to gene expression (GO:0010467), highlighting their potential alteration of this biological process. The GO term "cellular process (GO:0009987)" is present in

the sets of the two relatively more soluble compounds: IVj and IVk. This ontology covers a broad range of cellular processes, including cell-to-cell communication. The gen ontologies (Fig. 1(C)) associated to compound IVb–the hydrophobic compound lacking the nitro/amine-benzoxadiazole moiety–are related to those of IVa, sharing several GO terms related to metabolic processes, nitrogen compound biosynthesis, and organonitrogen compound biosynthesis. Additionally, IVb includes GO terms related to heterocycle biosynthesis.

Proteome Integral Solubility Alteration (PISA) and Determination of intracellular targets

The effectiveness of an antimicrobial agent is often determined by its ability to specifically interact with a cellular target of the microbe. Very few techniques have demonstrated the ability to identify targets at a system biology level. Here, the PISA assay has been used to identify intracellular targets for compound IV and its derivatives. This is the first time PISA assay, in the form of PISA-Express, has been successfully performed in living bacterial cells, with protocols adapted and modified from previous PISA studies in mammalian cells[16]. The experimental procedure involved exposing the bacteria to two different drug concentrations for 20 minutes. Afterwards, the cells in each sample were treated and split in two parts; one part was subjected to a temperature gradient and the other one was left without heating. Then, the soluble proteins were identified and quantified using mass spectrometry (Fig S1(C)). Because of the fast-doubling time of bacteria and related proteome expression changes even in a short time of incubation with compounds, the PISA assay was used in the PISA-Express form where PISA results on protein soluble amounts are normalized pairwise on the total protein abundance changes of the same samples relative to controls of PISA and expression assay.

We have observed several notable trends in the alteration of protein solubility. The top ten proteins with the most altered stability for each compound are listed in Fig 2(A). Three proteins stand out, CagA, HP_0542, and HP_0543, that are actively involved in the *cag* pathogenicity island renowned for its role in *H. pylori* virulence and for its association with an increased risk of gastric cancer[17]. Our observations indicate that all our compounds, except IVk, significantly affect the solubility of at least two out of the three above-mentioned proteins. Compounds IV (Fig 2(B-C)) and IVa (Fig 2(D-E)) specifically target CagA and HP_0542, while compound IVj (Fig. 2(H-I)) targets HP_0543 in addition to CagA. Only compound IVb (Fig. 2(F-G)) targets all three of these proteins. It is worth mentioning that, like other thermal proteome profiling-based assays, PISA

assay can identify changes in the solubility of specific target proteins and in that of the protein partners of their complex, as well as any other changes of solubility due to the altered complex formation and post-translational modifications. Changes in the solubility of multiple proteins within a specific complex strengthen the correlation between the drug and the complex itself. On the other hand, our PISA analysis has identified two proteins, FtsA and FtsZ, associated with the Z-ring formation in cell division that are affected by the compounds. Inhibition of Z ring formation has been a lucrative target for antimicrobial development. The orally bioavailable methylbenzamide antibiotic TXA-709 and its active metabolite TXA-707 target FtsZ and have been tested (phase I) against *Staphylococcus aureus*[16]. Compounds IV and IVb show a clear concentration-dependent targeting of both proteins (Fig S4(A and C)), while FtsZ and FtsA are additionally targeted by compounds IVa and IVj, respectively, albeit without a clear concentration dependency. Yet a third target that is shared among several compounds is the chaperone protein trigger factor (Tig), which plays a crucial role in facilitating proper protein folding and it is indispensable for the survival of the bacterial cells. This protein is targeted by all the compounds but IVk (Fig. 2(J-K)), in a concentration-dependent manner (Fig S4(B,D and E)).

We have also identified a few compound-specific proteins having altered stability. Compound IV strongly altered DNA-PolA and HP_1142, which function as DNA helicases, contributing to DNA replication and repair. Compounds IV and IVa altered the stability of PanD and CarA, which are both involved in the pantothenate biosynthesis pathway. Compound IVj targeted ArsR, HP_0543, HP_0853, LigA and RpsE, involved in interesting pathways. LigA is essential for DNA replication and repair while ArsR is a member of the two-component system ArsS/ArsR that regulates genes involved in biofilm formation and acid adaptation. Compound IVk is the only compound for which we could not detect any statistically significant altered protein with an adjusted p-value (adj.P.Val) of 0.001. However, compound IVk altered stability of several proteins with a relatively low adj.P.Val (0.005), as depicted in Figure S3(I-J). Notably, it does not share any of the previously described prominent potential targets.

Drugs interactions with essential proteins

Essential proteins have been primary targets for drug discovery. Reportedly, *H. pylori* possess 323 essential genes[19]. More than half of them is cytoplasmic and related to ribosomal proteins, while over 15% encode cell membrane proteins. The function of over 100 of these proteins remains unknown. We have looked for the interaction of our compounds with all 323 *H. pylori* essential proteins and we have detected 20

essential targets common for compounds IV, IVa, IVb and IVj (Fig. 3(A-H)), and not essential targets for IVk. It should be indicated that most of the unique proteins mentioned in this section are found in the PISA analysis but they are not in the top ten targets shown in Fig. 2(A)). The 20 common potential targets are mostly associated with cell division (for example, FtsZ), small subunit ribosomal proteins (RspC, RspE, RspL, RplE, InfC) and proteins associated with ATP production (AptD). Furthermore, we identified a few unique targets for compound IV (DnaN, involved in DNA tethering and processivity of DNA polymerases, and C694_06445, which could be a functional equivalent of delta subunit of DNA polymerase III). We also identified other essential proteins upon treatment with different compounds: for compound IVa (YlxH, involved in the placement and assembly of flagella); for compound IVb (AroK, shikimate kinase and AroC, shikimate synthase); and for compound IVj (AtpC, AtpF and AtpG, associated to F-ATPase, VepD, a very prominent target of virulence-associated protein d). Most interestingly, through our PISA analysis we have detected a clear interaction of compound IVj with flavodoxin (FldA), the protein that was used as initial *in vitro* target in the drug discovery process of compound IV, demonstrating the robustness of our experimental strategy.

Weighted Correlation Network Analysis and selection of drug-associated pathway

Weighted Correlation Network Analysis (WGCNA)[20] is a useful approach for constructing co-expression networks from high-dimensional omics data. One of the advantages of WGCNA is that the resulting co-expression networks are highly informative and can be used as a reference for downstream analyses of other types of omics data. Here we have used WGCNA to construct a scale-free signed network from the RNA-seq data. We have used topological overlap measures to merge genes into modules (Fig. 4(A)). We detected eight major gene modules and assigned distinct colors to each module for the ease of visualization and description (Fig. 4(A)). These modules were correlated with different compounds using Pearson correlation. Through p-value analysis, we identified the module that exhibited the strongest correlation with the compounds of interest (Fig. 4(B)). To understand the biological distribution of these modules we have looked for their overlap against the *H. pylori* protein-protein association network from the STRING database[21]. We divided the protein-protein association network into eight separate clusters using a method called "k-means". Each cluster represents a group of proteins that have similar levels of co-expression.

The color module "red" from WGCNA consists of 88 genes and shows up in different biological clusters (Fig. 4(C)). The hierarchical clustering of our compounds in this module reveals that compounds IVb and MNZ affect genes in this module differently from the control (Fig. 4(B) & S5(A)). The module "brown" forms the largest cluster, consisting of 420 genes. For this module, compounds IV, IVb, IVj and MNZ show down-regulation (Fig. 4(B) & S5(B)). We have not been able to detect any significant GO term enrichment from color module "magenta" but genes from this module are upregulated for compounds IV and IVj (Fig. 4(B) & S6(A)). Meanwhile, the color modules "greenyellow" (Fig. S6(B)) and "pink" (Fig. S7(A)). significantly associate with multiple GO terms related to chemotaxis and locomotion. The heatmaps show the upregulation of these genes associated with greenyellow and pink modules upon treatment with compound IVb and MNZ. Module "turquoise" includes 342 genes. This module is associated with the GO terms related to gene expression and translation among many other metabolic and biosynthetic processes (Fig. S6(B)). Genes from this module are downregulated by compounds IV, IVb, IVj and MNZ (Fig. 4(B) & S7(B)). The modules "black" and "turquoise" are closely related (Fig. 4(A)), but module "black" is specifically associated with ribosomes and protein-containing complexes (Fig. S8(A)). Compounds IV and IVj are the only ones that downregulate genes in this module (Fig. S8(A)). Finally, the module "purple" is linked to the pathogenesis and interspecies interaction (Fig. S8(B)). Compounds IV, IVk, and MNZ downregulate the genes associated with this pathway (Fig. 4(B) & S8(B)).

Identification of target-associated pathway

We have further integrated the modules identified through WGCNA into Cytoscape, a software platform for visualizing and analyzing complex networks. First, we linked the targets identified through the PISA assay with the modules that showed significant correlations in the WGCNA data. Next, to understand the pathway regulation associated with these targets, we merged the differential protein expression data with this network. This approach enables the detection of changes in gene co-expression associated with the target within a specific module. In addition, with this approach, it is possible to identify modules which are altered upon drug treatment even if they do not contain any prominent target. We hypothesized that the networks which lack any prominent target may be involved in the cellular response to a situation of stress.

We were able to identify two target groups in the module "brown". One group is associated with the virulence factor CagA, while the other is related to the cell division proteins FtsA and FtsZ. Module "brown" is positively correlated with compounds IV

and IVj and negatively correlated with compounds IVa (not significant) and IVk (Fig. 4(B)). In the same module, several drug targets were found to be related to compound IV (Fig. 5(A)) and, upon close inspection, we detected the down-regulation of multiple proteins related to CagA (Fig. S9(A)). Finally, module "brown" also includes a few essential protein targets like FtsA and ArsR.

The data from proteomics indicate the down-regulation of FtsY associated with FtsA (Fig. S9(B)). In the case of compound IVa, no modules were found to have a significant p-value. Therefore, we relied on correlation strength and analyzed the modules "brown" (Fig. 5(B)), "magenta", and "purple" in relation to this compound. Notably, we observed a very similar regulation of CagA in the case of compound IVa when compared to compound IV (Fig. S9(E)). However, the down-regulation of FtsY was not observed in this instance. Instead, we observed PolA and RecN as targets (Fig. S9(F)). It is worth mentioning that a single protein can be shared by closely related modules; in this instance, FtsA is present in both the modules "brown" and "pink". Compound IVb shows a significant correlation with the module "pink". We have detected FtsA as a potential target for compound IVb and in this analysis multiple proteins related to RNA processing, and associated with FtsA were found down-regulated in this module (Fig. 5(C)). Compound IVj shows five correlated modules and three of them are very similarly regulated modules compared to compound IV. In module "brown", we have detected six potential targets which include FtsA, PolA and CagA (Fig. 5(E)). Finally, while we have not detected any targets in module "pink" or "brown" associated with compound IVk, FtsA is up-regulated in both modules (Fig. S10(F and G)).

Compound IV does not have any target in the module "magenta", but RimP, which is involved in 30s ribosomal subunit maturation, is prominently down-regulated in this module (Fig. S9(C)). The module "black" associated with this compound contains Tig, which is involved in protein export, as a target, and it down-regulates multiple closely associated proteins (Fig. S9(D)). In the compound IVa-associated module "magenta", we identified ObgE, which is an essential GTPase, as a target (Fig. S9(G)). However, no specific target was detected for the module "purple", except for FliG, which is the flagellar motor switch protein. This protein was found to be down-regulated with compound IVa treatment (Fig. S9(H)). Protein ObgE is also one of the prominent candidate targets associated with compounds IVb and IVj in the module "magenta" and we have detected the down-regulation of multiple proteins related to ABC transporter (Fig. S10(B and D)). We have not identified any significant targets in the modules "purple", "greenyellow" and "red" that associate with compound IVb (Fig. S9(I and J) S10 (A)) and modules "purple", "black", "greenyellow" which associate with IVj

(Fig. S10(C-E)). In the case of compound IVk, we have detected four highly-correlated modules, including the module 'turquoise,' which is unique to this compound. Within these modules, we have identified seven potential targets, including helicase, RnhA, and GTPase Era (Fig. 5(F)). Module 'turquoise' is highly associated with gene expression, and the imbalance in differential transcripts and proteins may indicate transcriptional and translational decoupling, warranting further study for confirmation. Additionally, in modules 'brown' and 'red,' we have identified two potential targets as hypothetical proteins associated with compound IVk (Fig. S10(F-H)).

Biophysical assays to validate changes in targeted pathway

Elucidation of the mode of action of antimicrobial drugs has evolved in recent years. There is still considerable debate related to the role of reactive oxygen species (ROS) and their link to DNA damage in bactericidal drug-mediated antimicrobial activity. The investigation of the role of ROS as an overarching mode for bactericidal drug-mediated antimicrobial activity has led to some conflicting evidence either showing a common link between ROS and bactericidal drug-mediated antimicrobial activity[22], or demonstrating that the bactericidal activity does not depend on reactive oxygen species[23,24]. As our group of compounds exhibits a bactericidal behavior (Fig. 6(A)), we have looked for evidence of ROS generation. Compound IV and its derivatives cause a marked increase in ROS generation when compared to the control (DMSO). Though a degree of heterogenicity is expected due to the cellular stages, distribution and penetration of the drug at an early phase, compounds IV and IVj exhibit a broader change in ROS production (Fig. 6(B)). As described above, multiple DNA damage repair proteins are down-regulated in the presence of compounds IV, IVb and IVj. Also, DNA PolA was found to be a major target for compound IVj. Following these results, we have investigated compound-induced DNA damage by APO-BrdU TUNEL assay. All the compounds, particularly IV and IVj, caused significant DNA damage (Fig. 6(C)).

On the other hand, given that these drugs were developed as blockers for flavodoxin, and compound IVj clearly binds to this intercellular target, we have investigated the changes in oxygen consumption rate (OCR), since flavodoxin has been predicted to be part of the *H. pylori* electron transport chain. Though the signal-to-noise ratio of these data is considerable and further evaluation to quantify the amount of reduction in oxygen consumption is needed, the data suggest a reduction in OCR to a significant extent for compounds IV, IVa and IVj at corresponding MIC (Fig. 6(E)). Finally, we have

been able to detect a significant reduction in OCR at a higher concentration (2xMIC) of metronidazole and compound IVk.

Discussion

Multi-Omics have been extensively used in the understanding of host-pathogen interaction and microbiome studies but its full potential for determining antibacterial modes of action has not yet been explored. Modes of action of antibacterial compounds have been typically investigated using targeted experiments focusing on specific cellular processes or pathways, which may not capture the full complexity of antibacterial effects or potential resistance mechanisms. Our results show that multi-omics investigation combined with PISA is a useful tool for the discovery of new previously undetected drug-associated potential targets and for the validation of previously described ones.

We have used here a series of drugs that were initially developed to block *H. pylori* flavodoxin *in vitro* to showcase a multi-omics-based method for pathway deconvolution that can overcome two main challenges in pathway discovery. First, the detection of new potential targets for feature tailoring of an existing molecule, and second, the validation of the intracellular potential targets previously intended for a specific drug. Traditionally, the antimicrobial drug discovery process focused on identifying essential genes and proteins which could be targeted by inhibitory drugs discovered by phenotype screening. However, there is growing interest in non-essential genes or proteins involved in virulence, quorum sensing, biofilm formation or immune response evasion. This study identifies four out of our five compounds that strongly interact with CagA, the major virulence factor of *H. pylori*. The network analysis of CagA-associated proteins indicates systemic regulation and opens up new possibilities for exploring the efficacy of these drugs in the regulation of the type four secretion system. Nonetheless, all our compounds, except for compound IVk, additionally target multiple essential proteins. Among the most promising ones is FtsZ, a prominent target in three out of the five compounds tested. Although FtsA has not been categorized as essential, there is direct evidence for the localization of this protein at the cell division site. Along with FtsZ, we have identified FtsA as a potential target for compounds IV, IVb, and IVj. Our investigation into the systemic changes induced by this interaction spread across the WGCNA module 'brown' and module 'pink'. In the case of compounds IV and IVj, we have observed a positive correlation with module 'brown', and for compound IVb, a positive correlation with module 'pink'.

Another essential protein target that has been detected across the board is AtpD, a protein belonging to the ATP-synthase complex. In the case of compound IVj, we have detected four other potential targets from the ATP-synthase complex, namely AtpB, AtpC, AtpF, and AtpG along with AtpD. This poses IVj as a potentially effective ATP-synthase blocker. The ability of IV and IVj to inhibit ATP synthesis has been confirmed and demonstrated by a significant reduction in ATP production (see Fig. 6(D)).

Regarding the validation of the pre-defined target like flavodoxin, it is paramount to mention that some targets exhibit very limited shifts in solubility changes upon drug binding,[12,25,26] making the detection of the target difficult at a statistically significant level. In this regard, we have observed shifts in the solubility of flavodoxin for all the compounds, however, only in the case of compound IVj the change was statistically significant (Fig. S11). Other limitations of the target discovery process are the poor knowledge of the binding affinity of the compounds to their relative targets and the lack of any structural information about the potential binding site(s). At the methodological level, this research exemplifies the improved resolution of multi-omics data processing through the incorporation of the target deconvolution method. In summary, the study elucidates how the amalgamation of various techniques can foster a comprehensive grasp of intracellular events, thereby aiding in the advancement of antimicrobial drug development.

Methods

Culturing of *H. pylori*

H. pylori (ATCC 700392) was purchased from the American Type Culture Collection (ATCC, Manassas, VA, USA). Cultures of *H. pylori* were grown in brain heart infusion (BHI) broth (Oxoid) supplemented with 4% fetal bovine serum (FBS) (Pan-Biotech, Aidenbach, Germany) under microaerophilic conditions (85% N_2, 10% CO_2, 5% O_2) at 37 °C for 72 h. Prior to any assay, the absence of contaminations was verified using MALDI Biotyper® (MBT) microbial identification system.

Analysis for differentially expressed genes (Transcriptomics)

H. pylori (ATCC 700392) was grown as above and subjected to further incubation with compounds IV, IVa, IVb, IVj, IVk and metronidazol (MNZ) at their respective minimum inhibitory concentrations (MIC) for 4 h. Then, each *H. pylori* culture was washed three times with RNAlater (Sigma-Aldrich) for RNA extraction and library preparation and

stored at -80 °C. Three independent experiments were performed for each drug (Fig S1(B)). The samples were sequenced under Illumina NovaSeq, 2x150 bp configuration. After investigating the quality of the raw data, sequence reads were trimmed to remove possible adapter sequences and nucleotides with poor quality using Trimmomatic v.0.36. The trimmed reads were mapped to the *H. pylori* reference genome available on ENSEMBL using the STAR aligner v.2.5.2b[27]. Binary alignment and map (BAM) files were generated as a result of this step. Unique gene hit counts were calculated by using the feature Counts from the Subread package v.1.5.2[28]. Unique reads that fell within coding regions were counted. After the extraction of gene hit counts, the gene hit counts table was used for downstream differential expression analysis. A table of the top-ranked genes was extracted from a linear model fit using a Limma package[29]. Genes with adjusted p-values <0.001 and log fold change of >1 were defined as differentially expressed genes in each comparison.

To identify gene co-expression modules, we performed Weighted Correlation Network Analysis (WGCNA)[20] following the normalization of the data using the regularized log transform (rlog) function from the DESeq2 package[30]. A scale-free signed network was constructed with a power of 16, which was determined using the Soft Threshold selection method within WGCNA. Genes were then assigned to modules using topological overlap measures and closely related modules were merged based on their Eigengenes. Finally, we investigated correlations between modules and drugs using the Pearson correlation analysis.

Quantitative Proteomics of total protein amount changes

H. pylori (ATCC 700392) was grown as above and subjected to further incubation with compounds IV, IVa, IVb, IVj, IVk and metronidazol (MNZ) at their respected MIC for 4 h under the same conditions. Next, the *H. pylori* culture was washed three times with PBS to remove any residual protein from the culture media and cell pellets stored at -80 °C for protein extraction. The same bacterial mother flask was split into different flasks for producing biological replicates of compound treatment incubation, four for each condition. In order to include all samples, two 16-plex experiments were run with compounds IV, IVa and IVb in one plex, and IVj, IVk and MNZ in the other plex, both together with the same four replicates of DMSO control in each plex, used as identical peptide digested sample before tandem mass tag (TMT) labelling (Fig S1(C)). Briefly, samples extracted by incubation for 30 minutes at 23°C with PBS-based buffers containing 1x protease inhibitor, 50 µg/mL lysozyme, 250 U/mL benzonase, 1 mM MgCl2, and 0.4% NP40. The incubation was followed by adding the same volume of a

2×RIPA buffer, five freeze-thaw cycles using liquid nitrogen and 37°C, and ten 3s cycles of probe sonication on ice with 3s stop intervals. The total protein concentration of extracted samples was measured using micro-BCA assay and 50μM of protein was processed by dithiothreitol reduction, iodoacetamide alkylation, and cold acetone precipitation. Samples were resuspended in EPPS buffer, 8M urea, pH 8.0, diluted down to 4M urea and digested by LysC, then diluted down to 1M urea and digested with trypsin. Each digest was labelled using TMTpro 16-plex technology (Thermo Fischer) and a final multiplex sample was first cleaned by Sep-Pack C18 column (Waters). The final sample was fractionated off-line by capillary reversed phase chromatography at pH 10 into 12 fractions, and each of them was then analyzed by high-resolution nLC-ESI-MS/MS using an Orbitrap Exploris 480 instrument (Thermo Scientific). Peptide and protein identification, and quantification were carried out using Proteome Discoverer 2.5 (Thermo Scientific) with database search against the Uniprot database UP0000000429. Datasets were normalized on total TMT ion reporter intensity and on the average of DMSO controls. Then the normalized data were fitted to linear models using Limma[29] and differential expression proteins were selected compared to the DMSO controls.

Target deconvolution (PISA-Express assay)

H. pylori (ATCC 700392) was cultured as above for 72 hours. The culture was then incubated with compounds IV, IVa, IVb, IVj, and IVk at their respective minimum inhibitory concentrations (MIC) and five times the MIC for 20 minutes, also under the indicated microaerophilic conditions. For each compound, one PISA-Express experiment was carried out with 3 biological replicates of a control and each compound concentration. After the incubation, cells were pelleted at 7,000 × g for 5 minutes, washed with PBS, and centrifuged. The bacterial pellet was resuspended in 1.6 mL of PBS, and protease inhibitor. For each PISA experiment (Fig S1(D)), each replicate was divided into 16 aliquots of 55 µl each, which were processed at 16 different temperatures ranging from 46 to 70°C. The remaining volume in each tube was left for the expression proteomics control of each individual sample for total protein abundance in each individual PISA sample measured in its soluble protein abundance. Each expression proteomics control was treated similarly to the corresponding PISA sample, except for thermal treatment and ultracentrifugation. For each PISA sample, after thermal treatment, all temperatures of each replicate were combined and incubated for 30 minutes at 23°C, with the addition of 50 µg/mL

lysozyme, 250 U/mL benzonase, 1 mM $MgCl_2$, and 0.4% NP40. The incubation was followed by five freeze-thaw cycles using liquid nitrogen and 37°C. Ultracentrifugation was performed for 30 minutes at 125,000 × g at 4°C. The protein concentration of supernatants and protein extracts from the fraction of each sample not subjected to thermal treatment was measured using microBCA and 50 μg of total protein amount was processed as previously described for 18-plex PISA assay using TMTpro (Thermo Fisher)[15]. The final sample was fractionated off-line at high pH into 24 fractions, which were then run on nLC-ESI-MS/MS using a high-resolution Orbitrap Exploris 480 instrument.

Peptide and protein identification, and quantification were carried out using Proteome Discoverer 2.5 (Thermo Scientific) with database search against the Uniprot database UP0000000429. Datasets were normalized on total TMT ion reporter intensity and adjusted for batch effect using ComBat[31]. These normalized data were fitted to linear models using Limma[29] and differential expression proteins were selected compared to the DMSO controls.

Time-Kill Curves

H. pylori (ATCC 700392) was grown as above at a final cell density of 10^5 cells/mL. A sample of 2.5 mL of this pre-inoculum were transferred to each well of a 24-well plate. The culture was subjected to incubation with compounds IV, IVa, IVb, IVj and IVk at their respected MIC for 24 h. At every time point, 20 μL from each condition were sampled from 24-well plate and serially 10-fold diluted in 180 μL of phosphate-buffered saline (PBS) (Millipore) Then, 2.5 μL of each diluted and non-diluted sample were plated on blood agar plates. Colony forming units (CFU) were determined by colony counting after 5 days of incubation. Experiments were performed in duplicate and repeated at least twice.

Cellular reactive oxygen species (ROS) assay

The relative amount of intracellular ROS was quantified by using the cell-permeable fluorescent probe 2′,7′-dichlorofluorescin diacetate (DCFDA), which gets de-esterified intracellularly and turns to highly fluorescent 2′,7′-dichlorofluorescein upon oxidation. *H. pylori* was grown for 72 h with agitation under microaerophilic conditions (85% N_2, 10% CO_2, 5% O_2), harvested, and washed with PBS. Cells were resuspended until a final density of 0.1 in Gibco FluoroBrite DMEM media supplemented with DCFDA (5 μM). After 30 min of pre-incubation at 37 °C, compounds IV, IVa, IVb, IVj, IVk, MNZ (at their respective MIC) and 20 μM H_2O_2 were added, and the fluorescence was measured

using a Beckman Coulter flow cytometry system. The DCFDA probe, upon oxidation, emits fluorescent signals that are indicative of intracellular ROS levels. To ensure reliability and generate statistically significant data, the experiment was performed three times independently. The data obtained from each experiment were merged, and ggplot, a data visualization package in the R programming language, was used to visualize the results.

Compound-induced DNA damage assay

H. pylori was grown for 72 h with agitation under microaerophilic conditions harvested and washed with PBS. Cells were resuspended until a final density of 0.6 in Gibco FluoroBrite DMEM media supplemented with DCFDA (5 µM). After 30 min pre-incubation at 37 °C, compounds IV, IVa, IVb, IVj, IVk, MNZ (at their respective MIC) and 20 µM H_2O_2 were added and kept for 24 h at 37 °C under microaerophilic conditions. Next, cells were labelled according to the Apo-direct BD kit protocol. To detect compound induced DNA breaks, reagent TdT (which attach a bromolated deoxyuridine triphosphate (Br-dUTP) molecule to the damaged DNA that have a free hydroxyl (OH) group) was added to the cells. After treatment with Br-dUTP, the cells were stained with a fluorescent FITC-labeled anti-BrdU monoclonal antibody. This stain helps visualize the damaged DNA in the cells. The cells were then analyzed using flow cytometry.

Measurement of ATP depletion in *Helicobacter pylori*

The ATP depletion in *H.pylori* cells was assessed using a luminescence-based method. Specifically, the BacTiter-Glo microbial cell viability assay kit (Promega, USA) was employed for this purpose. The assay was performed following the manufacturer's instructions. To prepare the BacTiter-Glo reagent, the lyophilized BacTiter-Glo enzyme/substrate mixture was combined with the buffer at room temperature. Separate wells of an opaque-walled 96-well microplate were designated for the drug-treated *Helicobacter pylori* culture and the control (DMSO). One hundred microliters of the drug-treated culture and the untreated control were added to their respective wells. Next, 100 µL of the prepared BacTiter-Glo reagent was added to each well containing the *H. pylori* culture and control. The contents were gently mixed and incubated in the dark for 5 minutes to allow for cell lysis and ATP release. Following the incubation period, luminescence intensity was measured using a Varioskan™ LUX multimode microplate reader (Thermo Fisher, USA). The luminescence signal is directly proportional to the amount of ATP present in the sample. A decrease in luminescence intensity in the drug-treated samples compared to the untreated control indicates ATP

depletion in the *H. pylori* cells after the 2-hour incubation with the drug. The relative ATP depletion can be calculated as the percentage decrease in luminescence compared to the untreated control.

Measurement of Oxygen Consumption Rate (OCR)

Cellular oxygen consumption rate (OCR) was measured using the extracellular flux analyzer XFe96 (from Seahorse Bioscience at the MOSBRI EU Infrastructure - HypACB facility at Sapienza University) To reproduce the biological condition in the stomach, where oxygen levels are relatively low this assay was conducted under hypoxic conditions[32]. *H. pylori* cells were cultured in BHI at 37 °C (HypoxicLab, Oxford Optronic- 95% N2, 5% O2, 10% CO2, 20% humidity), then transferred into the Don Whitley (i2 workstation) hypoxic chamber (95% N2, 5% O2, 20% humidity), where cellular oxygen consumption rate (OCR) was measured.

The sensor cartridge for Seahorse was hydrated at 37 °C a day before each experiment, following the manufacturer's instructions, under hypoxic conditions. Before cell seeding, the Seahorse 96-well plates were coated by adding 20 µL of a 1x collagen solution in each well, which was prepared from a 20x stock type I solution (Sigma C3867-1VL). After 1 hour, the collagen solution was removed, and the wells were left to dry under a laminar flow hood. The last column of the plate was not coated since it contained the medium alone to allow the addition of sodium sulfite (VWR 0628-500g) during the run. Sodium sulfite (100 mM final concentration) was used as a chemical oxygen scavenger to provide a "zero" oxygen reference. Coating plus medium was used to measure the environmental oxygen levels as a reference during the experiment. The injection ports containing the different stressors/additives (i.e., 10x DMSO, 10x stock drugs, or 10x sulfite) were loaded (20 µL per well) in the Seahorse chamber, 1 hour before the Seahorse run.

Exponentially growing *H. pylori* cells were harvested by centrifugation (10 minutes at 4000 rpm) and resuspended in the growth chamber with Seahorse medium (supplemented with 10 mM glucose, 1 mM pyruvate, and 2 mM glutamine, following the manufacturer's instructions) to achieve a final OD600 of 0.6. The cells were then seeded on the collagen-coated plate (180 µL per well), except for the last column, and vortexed. After a Seahorse calibration run, the cell plate was loaded into the instrument following the manufacturer's instructions.

Measurements were set as follows: 3 minutes of mixing, where the plate well was allowed to exchange gases with the hypoxic environment, followed by 3 minutes of

measurements. During the 3-minute measurement, the 96 probes protruding from the lid were automatically inserted into the cell plate, creating a microchamber per well. This transiently sealed microchamber allowed the instrument to measure the oxygen consumption carried out by the cell monolayer without any gas exchange with the environment. After 6 baseline measurements, the drug/sulfite was automatically added to each well, as indicated. Kinetics were considered for the first hour to avoid any bias due to cell stress or excessive metabolic activity.

To compare the different OCR obtained from independent experiments, relative values have been used as follows: OCR of each sample (with 6 replicates) at 60 minutes was related to the basal OCR and compared with the same ratio obtained with the sole DMSO (as the untreated reference sample). Values are the means of the replicates ±SD.

Data Availability

Maity, Ritwik, Zhang, Xuepei, Romana Liberati , Francesca, Cutruzzolà, Francesca, Rinaldo, Serena, Gaetani, Massimiliano, Antonio Aínsa, José, & Sancho, Javier. (2023). Dataset for publication: Merging Multi-OMICs with Proteome Integral Solubility Alteration Unveils Antibiotic Mode of Action [Data set]. Zenodo. https://doi.org/10.5281/zenodo.8321088

Acknowledgement

Full support in the experimental design, performance, and data analysis of the proteomic study was provided by the "Chemical Proteomics" Unit of Karolinska Institutet (KI) within the Division of Chemistry I at the Department of Medical Biochemistry and Biophysics. Chemical Proteomics is a KI core facility, a national unit of SciLifeLab and a national node of the Swedish National Infrastructure for Biological Mass Spectrometry (BioMS). We would also like to express our gratitude to Dr. Ana Isabel López and her team at Hospital Universitario Miguel Servet, Zaragoza, as well as Prof. Volkan Özenci and Ramona Santini at Karolinska Institutet, for their continuous assistance in verifying microbial samples using the MALDI Biotyper® (MBT) microbial identification system. This project has received funding from the European Union´s H2020 research and innovation programme under Maria Sklodowska-Curie grant agreement No 801586 and the European Union's Horizon 2020 research and innovation programme under grant agreement No 101004806. We acknowledge

financial support to JS from FLAV4AMR (JPIAMR), PID2019-309 107293GB-I00 (MICINN, Spain) and E45_23R (Gobierno de Aragón, Spain).

References

1. Murray, C. J. L. *et al.* Global burden of bacterial antimicrobial resistance in 2019: a systematic analysis. *The Lancet* **399**, 629–655 (2022).

2. WHO publishes list of bacteria for which new antibiotics are urgently needed. https://www.who.int/news/item/27-02-2017-who-publishes-list-of-bacteria-for-which-new-antibiotics-are-urgently-needed.

3. Zamani, M. *et al.* Systematic review with meta-analysis: the worldwide prevalence of Helicobacter pylori infection. *Aliment. Pharmacol. Ther.* **47**, 868–876 (2018).

4. Ho, J. J. C., Navarro, M., Sawyer, K., Elfanagely, Y. & Moss, S. F. Helicobacter pylori Antibiotic Resistance in the United States Between 2011 and 2021: A Systematic Review and Meta-Analysis. *Off. J. Am. Coll. Gastroenterol. ACG* **117**, 1221 (2022).

5. Salillas, S. *et al.* Selective Targeting of Human and Animal Pathogens of the Helicobacter Genus by Flavodoxin Inhibitors: Efficacy, Synergy, Resistance and Mechanistic Studies. *Int. J. Mol. Sci.* **22**, 10137 (2021).

6. Cunha, E. S., Chen, X., Sanz-Gaitero, M., Mills, D. J. & Luecke, H. Cryo-EM structure of Helicobacter pylori urease with an inhibitor in the active site at 2.0 Å resolution. *Nat. Commun.* **12**, 230 (2021).

7. Lettl, C. *et al.* Selective killing of the human gastric pathogen Helicobacter pylori by mitochondrial respiratory complex I inhibitors. *Cell Chem. Biol.* **30**, 499-512.e5 (2023).

8. Salillas, S. *et al.* Design, Synthesis, and Efficacy Testing of Nitroethylene- and 7-Nitrobenzoxadiazol-Based Flavodoxin Inhibitors against Helicobacter pylori Drug-Resistant Clinical Strains and in Helicobacter pylori-Infected Mice. *J. Med. Chem.* **62**, 6102–6115 (2019).

9. Iwata, M., Sawada, R., Iwata, H., Kotera, M. & Yamanishi, Y. Elucidating the modes of action for bioactive compounds in a cell-specific manner by large-scale chemically-induced transcriptomics. *Sci. Rep.* **7**, 40164 (2017).

10. Santos, R. *et al.* A comprehensive map of molecular drug targets. *Nat. Rev. Drug Discov.* **16**, 19–34 (2017).

11. Heppler, L. N. *et al.* The antimicrobial drug pyrimethamine inhibits STAT3 transcriptional activity by targeting the enzyme dihydrofolate reductase. *J. Biol. Chem.* **298**, (2022).

12. Molina, D. M. *et al.* Monitoring Drug Target Engagement in Cells and Tissues Using the Cellular Thermal Shift Assay. *Science* **341**, 84–87 (2013).

13. Gaetani, M. & Zubarev, R. A. Proteome Integral Solubility Alteration (PISA) for High-Throughput Ligand Target Deconvolution with Increased Statistical Significance and Reduced Sample Amount. in *Cell-Wide Identification of Metabolite-Protein Interactions* (eds. Skirycz, A., Luzarowski, M. & Ewald, J. C.) 91–106 (Springer US, 2023). doi:10.1007/978-1-0716-2624-5_7.

14. Gaetani, M. *et al.* Proteome Integral Solubility Alteration: A High-Throughput Proteomics Assay for Target Deconvolution. *J. Proteome Res.* **18**, 4027–4037 (2019).

15. Proteome Integral Solubility Alteration (PISA) Assay in Mammalian Cells for Deep, High-Confidence, and High-Throughput Target Deconvolution. https://en.bio-protocol.org/en/bpdetail?id=4556&type=0.

16. Sabatier, P. *et al.* An integrative proteomics method identifies a regulator of translation during stem cell maintenance and differentiation. *Nat. Commun.* **12**, 6558 (2021).

17. Parsonnet, J., Friedman, G. D., Orentreich, N. & Vogelman, H. Risk for gastric cancer in people with CagA positive or CagA negative Helicobacter pylori infection. *Gut* **40**, 297–301 (1997).

18. Lepak, A. J. *et al.* In Vivo Pharmacodynamic Evaluation of an FtsZ Inhibitor, TXA-709, and Its Active Metabolite, TXA-707, in a Murine Neutropenic Thigh Infection Model. *Antimicrob. Agents Chemother.* **59**, 6568–6574 (2015).

19. Salama, N. R., Shepherd, B. & Falkow, S. Global Transposon Mutagenesis and Essential Gene Analysis of Helicobacter pylori. *J. Bacteriol.* **186**, 7926–7935 (2004).

20. Langfelder, P. & Horvath, S. WGCNA: an R package for weighted correlation network analysis. *BMC Bioinformatics* **9**, 559 (2008).

21. Szklarczyk, D. *et al.* The STRING database in 2023: protein-protein association networks and functional enrichment analyses for any sequenced genome of interest. *Nucleic Acids Res.* **51**, D638–D646 (2023).

22. Kohanski, M. A., Dwyer, D. J., Hayete, B., Lawrence, C. A. & Collins, J. J. A Common Mechanism of Cellular Death Induced by Bactericidal Antibiotics. *Cell* **130**, 797–810 (2007).

23. Keren, I., Wu, Y., Inocencio, J., Mulcahy, L. R. & Lewis, K. Killing by Bactericidal Antibiotics Does Not Depend on Reactive Oxygen Species. *Science* **339**, 1213–1216 (2013).

24. Liu, Y. & Imlay, J. A. Cell Death from Antibiotics Without the Involvement of Reactive Oxygen Species. *Science* **339**, 1210–1213 (2013).

25. Sabatier, P., Beusch, C. M., Meng, Z. & Zubarev, R. A. System-Wide Profiling by Proteome Integral Solubility Alteration Assay of Drug Residence Times for Target Characterization. *Anal. Chem.* **94**, 15772–15780 (2022).

26. Savitski, M. M. *et al.* Tracking cancer drugs in living cells by thermal profiling of the proteome. *Science* **346**, 1255784 (2014).

27. Dobin, A. *et al.* STAR: ultrafast universal RNA-seq aligner. *Bioinformatics* **29**, 15–21 (2013).

28. Liao, Y., Smyth, G. K. & Shi, W. The Subread aligner: fast, accurate and scalable read mapping by seed-and-vote. *Nucleic Acids Res.* **41**, e108 (2013).

29. limma powers differential expression analyses for RNA-sequencing and microarray studies | Nucleic Acids Research | Oxford Academic. https://academic.oup.com/nar/article/43/7/e47/2414268.

30. Moderated estimation of fold change and dispersion for RNA-seq data with DESeq2 | Genome Biology | Full Text. https://genomebiology.biomedcentral.com/articles/10.1186/s13059-014-0550-8.

31. Zhang, Y., Parmigiani, G. & Johnson, W. E. ComBat-seq: batch effect adjustment for RNA-seq count data. *NAR Genomics Bioinforma.* **2**, lqaa078 (2020).

32. Abass, A. *et al.* Effect of low oxygen concentration on activation of inflammation by Helicobacter pylori. *Biochem. Biophys. Res. Commun.* **560**, 179–185 (2021).

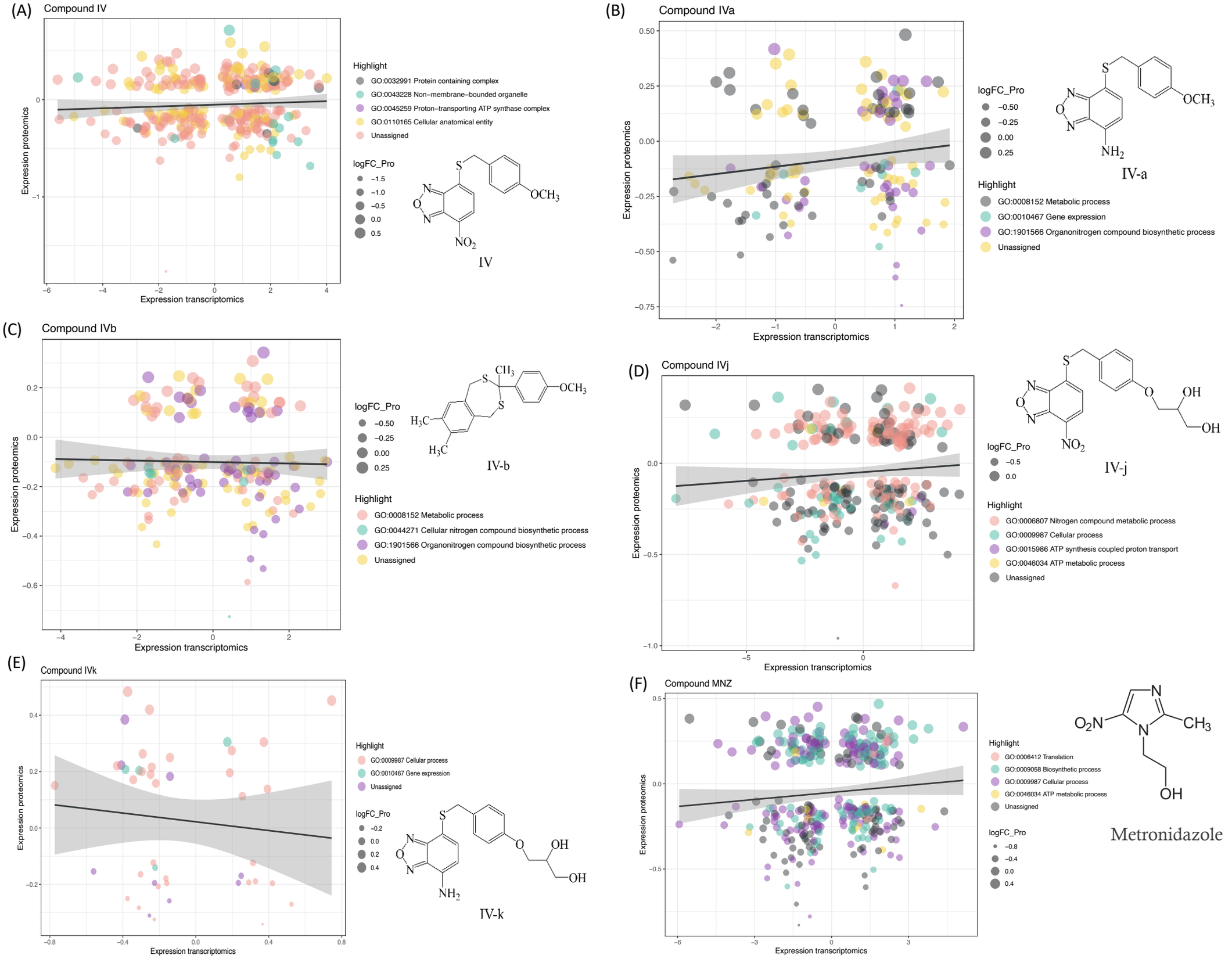
(A)
Compound IV
Expression proteomics
Expression transcriptomics
Highlight
GO:0032991 Protein containing complex
GO:0043228 Non−membrane−bounded organelle
GO:0045259 Proton−transporting ATP synthase complex
GO:0110165 Cellular anatomical entity
Unassigned
logFC_Pro
−1.5
−1.0
−0.5
0.0
0.5
IV
(B)
Compound IVa
Expression proteomics
Expression transcriptomics
logFC_Pro
−0.50
−0.25
0.00
0.25
IV-a
Highlight
GO:0008152 Metabolic process
GO:0010467 Gene expression
GO:1901566 Organonitrogen compound biosynthetic process
Unassigned
(C)
Compound IVb
Expression proteomics
Expression transcriptomics
logFC_Pro
−0.50
−0.25
0.00
0.25
IV-b
Highlight
GO:0008152 Metabolic process
GO:0044271 Cellular nitrogen compound biosynthetic process
GO:1901566 Organonitrogen compound biosynthetic process
Unassigned
(D)
Compound IVj
Expression proteomics
Expression transcriptomics
logFC_Pro
−0.5
0.0
IV-j
Highlight
GO:0006807 Nitrogen compound metabolic process
GO:0009987 Cellular process
GO:0015986 ATP synthesis coupled proton transport
GO:0046034 ATP metabolic process
Unassigned
(E)
Compound IVk
Expression proteomics
Expression transcriptomics
Highlight
GO:0009987 Cellular process
GO:0010467 Gene expression
Unassigned
logFC_Pro
−0.2
0.0
0.2
0.4
IV-k
(F)
Compound MNZ
Expression proteomics
Expression transcriptomics
Highlight
GO:0006412 Translation
GO:0009058 Biosynthetic process
GO:0009987 Cellular process
GO:0046034 ATP metabolic process
Unassigned
logFC_Pro
−0.8
−0.4
0.0
0.4
Metronidazole

Fig. 1 Changes in the transcriptomics and proteomics landscape, along with the associated gene ontology. (A-F) These panels highlight the common genes and proteins associated with individual compounds, with different colors indicating the distribution of these genes and proteins across various gene ontology terms.

(A) Proteins with highest solubility alteration

Compound	Targets									
Compound IV	cagA	carA	ftsA	HP_0542	HP_0706	HP_0853	HP_1142	panD	rpsA	tig
Compound IVa	cagA	carA	dnaJ	HP_0486	HP_0542	HP_1236	obg	rpsA	tig	ychF
Compound IVb	cagA	dnaJ	ftsA	HP_0486	HP_0542	HP_0543	HP_0706	rpsA	tig	ychF
Compound IVj	arsR	cagA	dnaJ	ftsA	HP_0543	HP_0853	ligA	rpsA	rpsE	tig
Compound IVk	amiF	HP_0750	HP_0803	HP_0922	HP_0993	HP_1091	HP_1163	HP_1276	HP_1390	rnhA

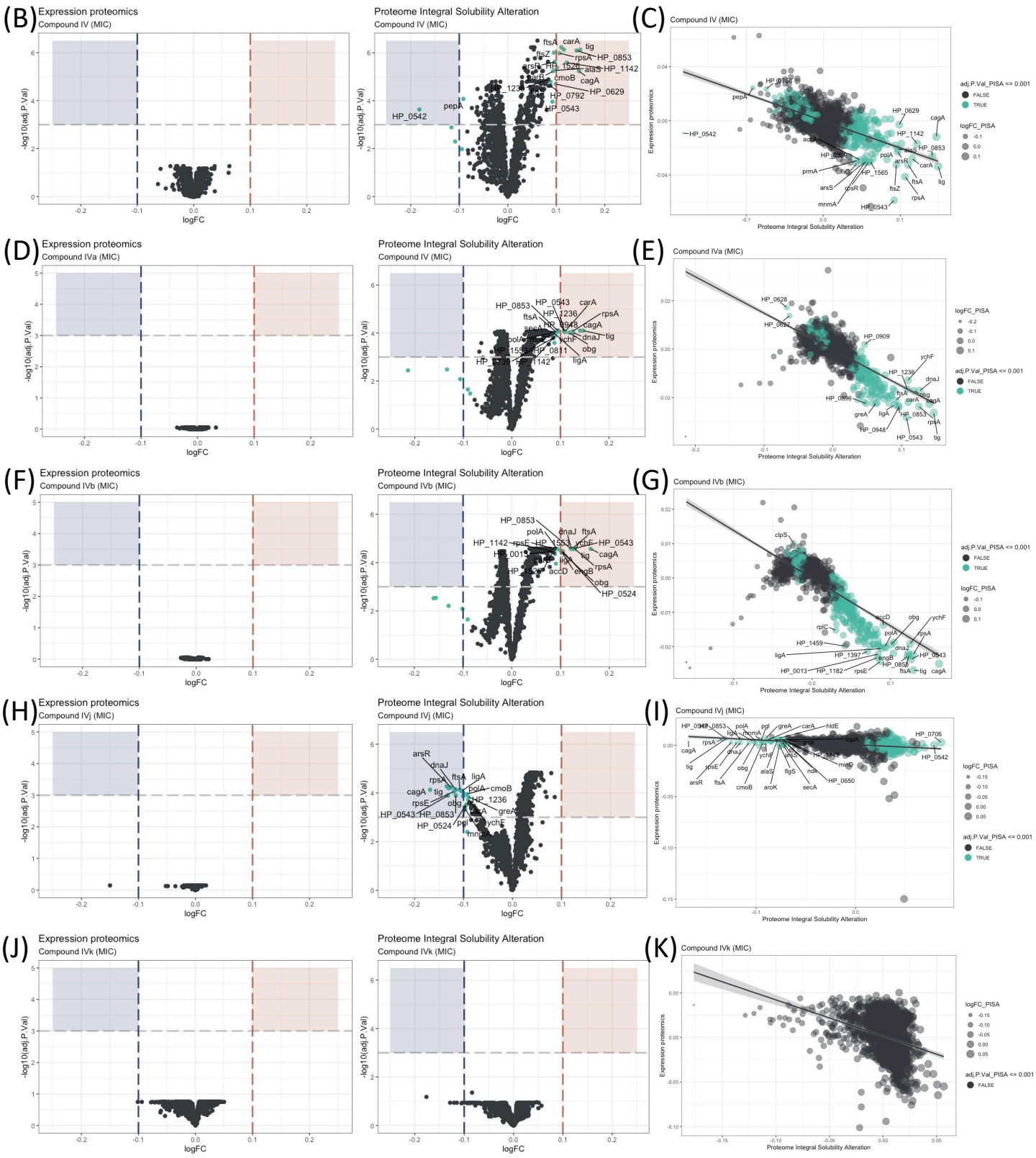

Fig. 2: Proteome Integral Solubility Alteration (PISA) analysis and intracellular target determination.

(A) Table of the top 10 intracellular targets and their corresponding minimal inhibitory concentrations (MIC) for individual compounds.
(B) Volcano plot of significant alterations in protein solubility for Compound IV at its MIC.
(C) Scatterplot demonstrating significant alterations (teal color) in protein solubility for Compound IV compared to baseline protein expression changes.
(D) Volcano plot of significant alterations in protein solubility for Compound IVa at its MIC.
(E) Scatterplot presenting significant alterations (teal color) in protein solubility for Compound IVa compared to baseline protein expression changes.
(F) Volcano plot of significant alterations in protein solubility for Compound IVb at its MIC.
(G) Scatterplot indicating significant alterations (teal color) in protein solubility for Compound IVb compared to baseline protein expression changes.
(H) Volcano plot of significant alterations in protein solubility for Compound IVj at its MIC.
(I) Scatterplot highlighting significant alterations (teal color) in protein solubility for Compound IVj compared to baseline protein expression changes.
(J) Volcano plot no significant alterations in protein solubility for Compound IVk at its MIC.
(K) Scatterplot presenting no significant alterations in protein solubility for Compound IVk compared to baseline protein expression changes.

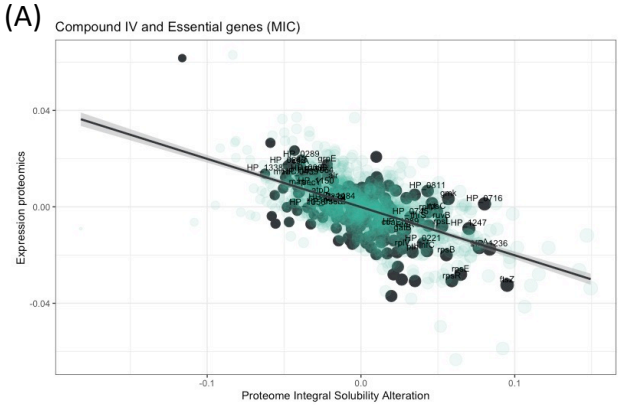

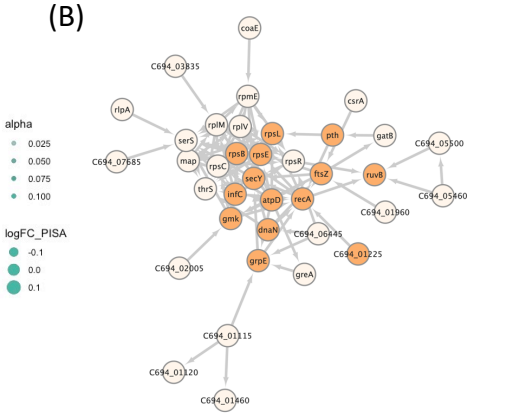

GO:0006412
Translation

GO:0010467
Gene expression

GO:0044267
Cellular protein metabolic process

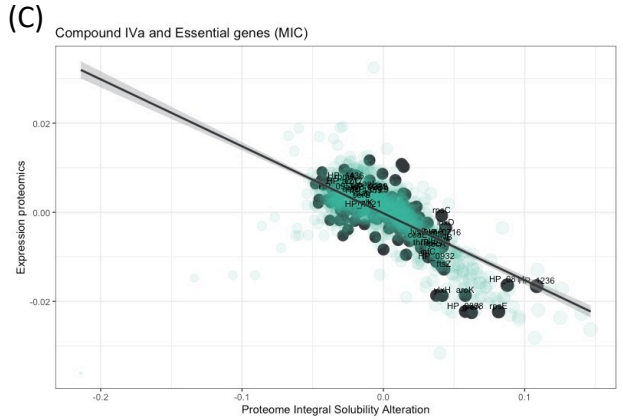

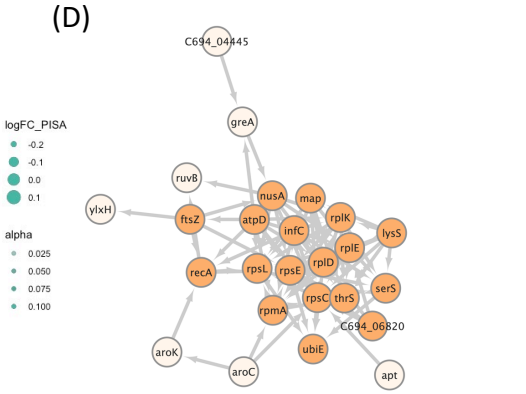

GO:0006412
Translation

GO:0010467
Gene expression

GO:0044249
Cellular biosynthetic process

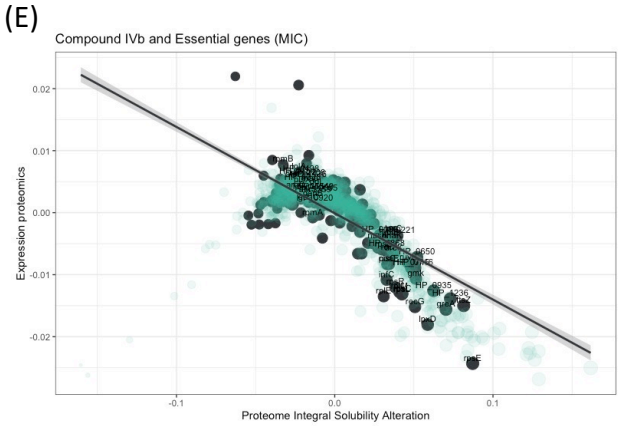

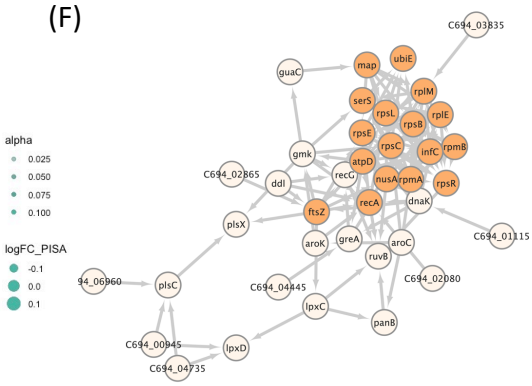

GO:0006412
Translation

GO:0010467
Gene expression

GO:0043604
Amide biosynthetic process

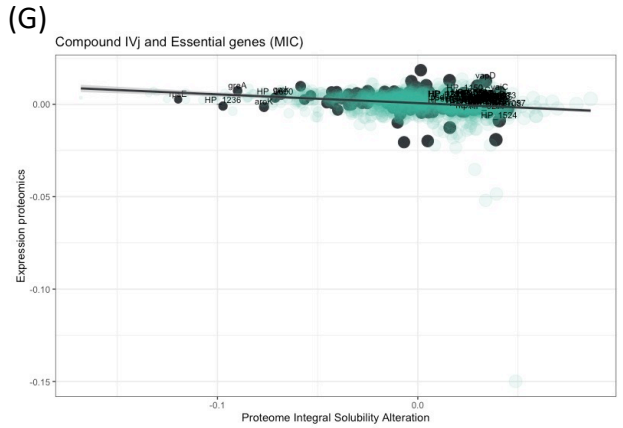

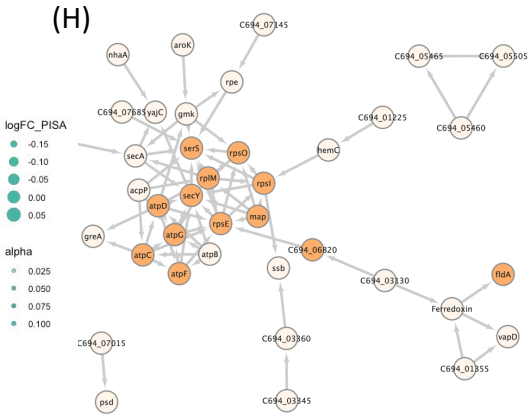

GO:0015078
Proton transmembrane transporter activity

GO:0046933
Proton-transporting ATP synthase activity

GO:0045259
Proton-transporting ATP synthase complex

Fig. 3 Interactions of drugs with essential proteins.

(A) The intracellular essential protein targets detected for compound IV. The data highlights significant alterations (shown in black) in protein solubility compared to the baseline protein expression changes.

(B) Protein co-expression network among the essential proteins with significant alterations by the compound IV. Highlighted nodes indicate the distribution of the first Gene Ontology (GO) term associated with these proteins.

(C) Protein targets detected for compound IVa are presented. The data highlights significant alterations (shown in black) in protein solubility compared to the baseline protein expression changes.

(D) Protein co-expression network among the essential proteins with significant alterations by the compound IVa . Highlighted nodes indicate the distribution of the first Gene Ontology (GO) term associated with these proteins.

(E) The intracellular essential protein targets detected for compound IVb are presented. The data highlights significant alterations (shown in black) in protein solubility compared to the baseline protein expression changes.

(F) Protein co-expression network among the essential proteins with significant alterations by the compound IVb. Highlighted nodes indicate the distribution of the first Gene Ontology (GO) term associated with these proteins.

(G) The intracellular essential protein targets detected for compound IVj are presented. The data highlights significant alterations (shown in black) in protein solubility compared to the baseline protein expression changes.

(H) The figure illustrates the protein co-expression network among the essential proteins with significant alterations for compound IVj . Highlighted nodes indicate the distribution of the first Gene Ontology (GO) term associated with these proteins.

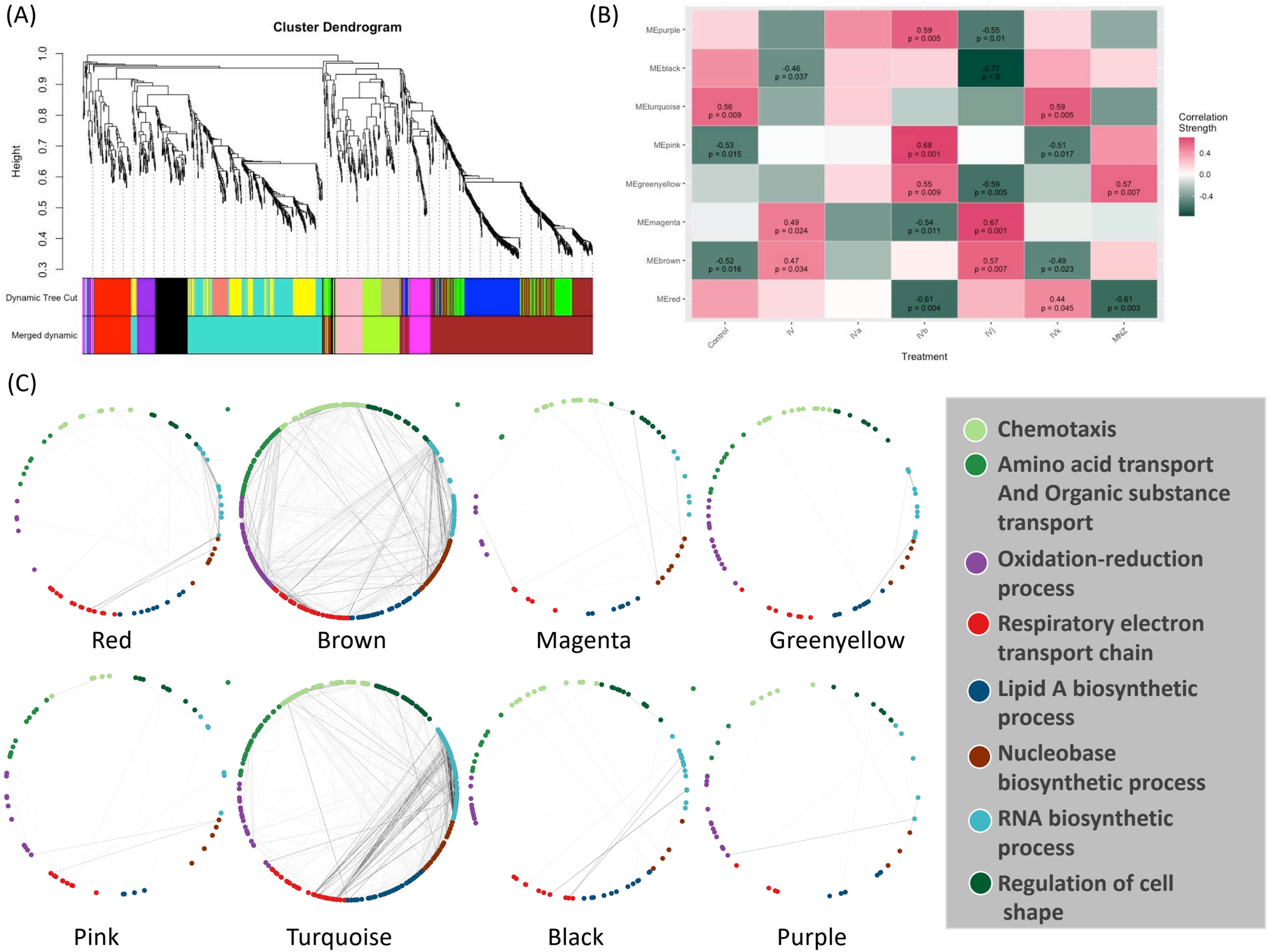
(A)
Cluster Dendrogram
Height
1.0
0.9
0.8
0.7
0.6
0.5
0.4
0.3
Dynamic Tree Cut
Merged dynamic
(B)
MEpurple
MEblack
MEturquoise
MEpink
MEgreenyellow
MEmagenta
MEbrown
MEred
0.59 p = 0.005
-0.55 p = 0.01
-0.46 p = 0.037
-0.77 p = 0
0.56 p = 0.009
0.59 p = 0.005
-0.53 p = 0.015
0.68 p = 0.001
-0.51 p = 0.017
0.55 p = 0.009
-0.59 p = 0.005
0.57 p = 0.007
0.49 p = 0.024
-0.54 p = 0.011
0.67 p = 0.001
-0.52 p = 0.016
0.47 p = 0.034
0.57 p = 0.007
-0.49 p = 0.023
-0.61 p = 0.004
0.44 p = 0.045
-0.61 p = 0.003
Control
IV
IVa
IVb
IVj
IVk
MNZ
Treatment
Correlation Strength
0.4
0.0
-0.4
(C)
Red
Brown
Magenta
Greenyellow
Pink
Turquoise
Black
Purple
Chemotaxis
Amino acid transport And Organic substance transport
Oxidation-reduction process
Respiratory electron transport chain
Lipid A biosynthetic process
Nucleobase biosynthetic process
RNA biosynthetic process
Regulation of cell shape

Fig. 4 Weighted Correlation Network Analysis (WGCNA) and the selection of drug-associated pathways.

(A) The clustering dendrogram and expression heatmap of genes are presented, identifying the WGCNA modules.
(B) The correlation between the identified modules and different treatments is displayed. Modules that exhibit a significant association with traits, indicated by a correlation greater than 0.5 and a p-value less than 0.05, are denoted by an asterisk (*). Red and green colors represent positive and negative correlations with gene expression, respectively.
(C) The distribution of different WGCNA modules within the protein co-expression network of H. pylori is depicted.

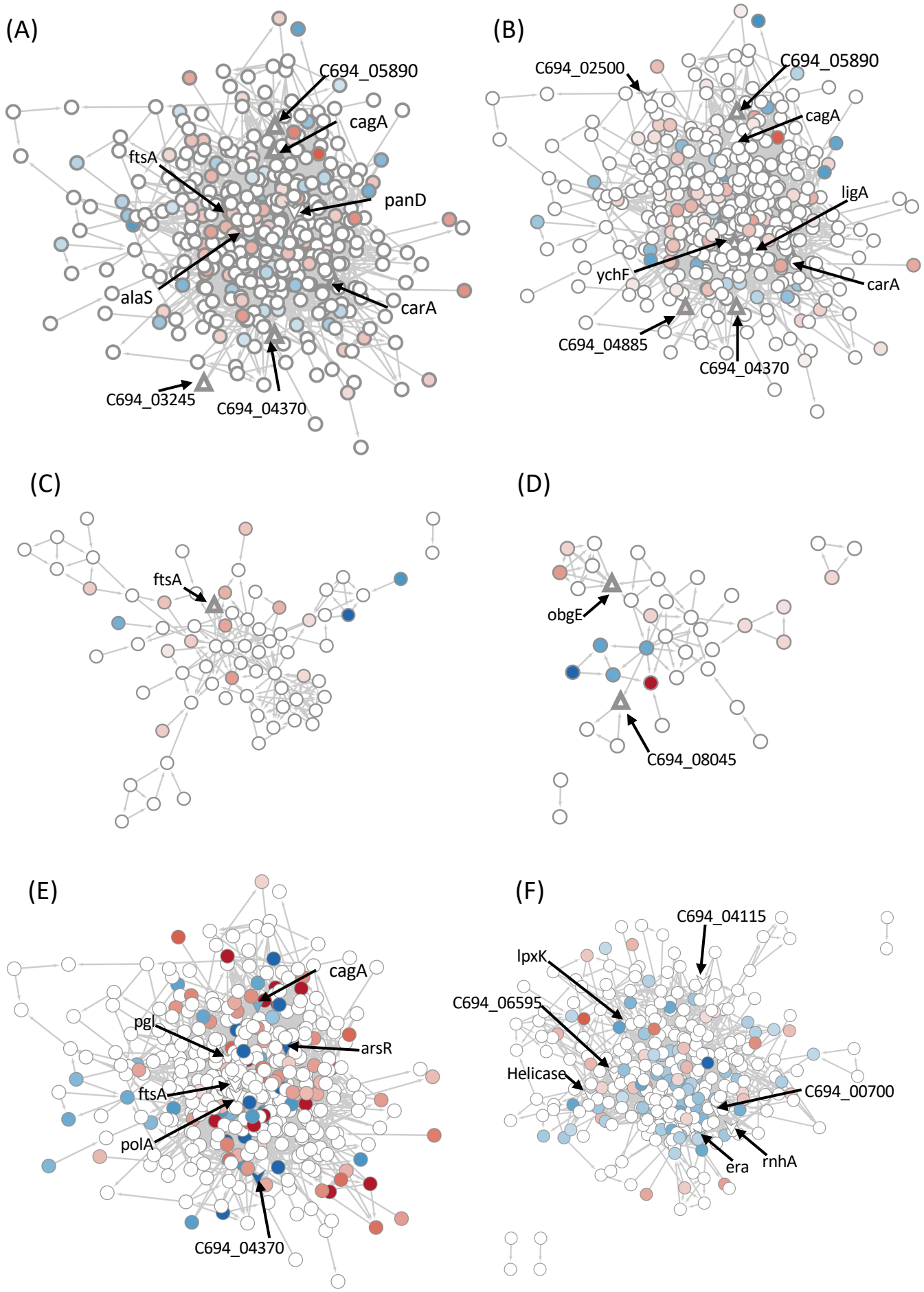
(A)
C694_05890
cagA
ftsA
panD
alaS
carA
C694_03245
C694_04370
(B)
C694_02500
C694_05890
cagA
ligA
ychF
carA
C694_04885
C694_04370
(C)
ftsA
(D)
obgE
C694_08045
(E)
cagA
pgl
arsR
ftsA
polA
C694_04370
(F)
C694_04115
lpxK
C694_06595
Helicase
C694_00700
era
rnhA

Fig. 5 Identification of target-associated pathways.
(A) Differential expression of proteins influenced by Compound IV. Upregulated proteins are represented in red, while downregulated proteins are represented in blue. The targets associated with Compound IV are highlighted within the brown module.
(B) Differential expression of proteins influenced by Compound IVa. Upregulated proteins are represented in red, while downregulated proteins are represented in blue. The targets associated with Compound IVa are highlighted within the brown module.
(C) Differential expression of proteins influenced by Compound IVb. Upregulated proteins are represented in red, while downregulated proteins are represented in blue. The targets associated with Compound IVb are highlighted within the pink module.
(D) Differential expression of proteins influenced by Compound IVb. Upregulated proteins are represented in red, while downregulated proteins are represented in blue. The targets associated with Compound IVb are highlighted within the megenta module.
(E) Differential expression of proteins influenced by Compound IVj. Upregulated proteins are represented in red, while downregulated proteins are represented in blue. The targets associated with Compound IVj are highlighted within the brown module.
(F) Differential expression of proteins influenced by Compound IVk. Upregulated proteins are represented in red, while downregulated proteins are represented in blue. The targets associated with Compound IVk are highlighted within the turquoise module.

(A)

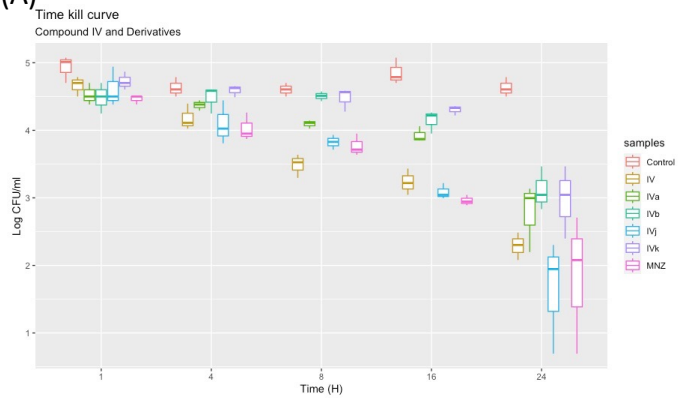
Time kill curve
Compound IV and Derivatives
Log CFU/ml
Time (H)
samples
Control
IV
IVa
IVb
IVj
IVk
MNZ

(B)

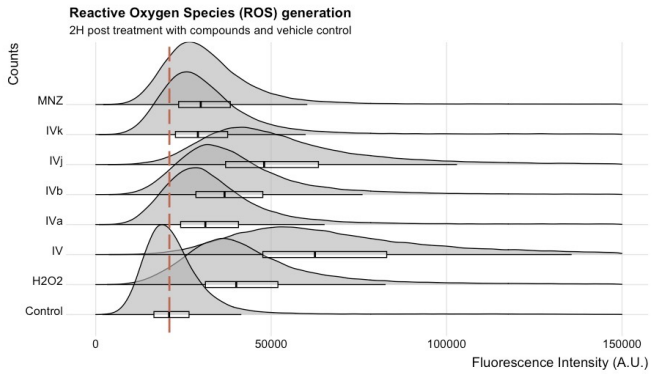
Reactive Oxygen Species (ROS) generation
2H post treatment with compounds and vehicle control
Counts
MNZ
IVk
IVj
IVb
IVa
IV
H2O2
Control
Fluorescence Intensity (A.U.)

(C)

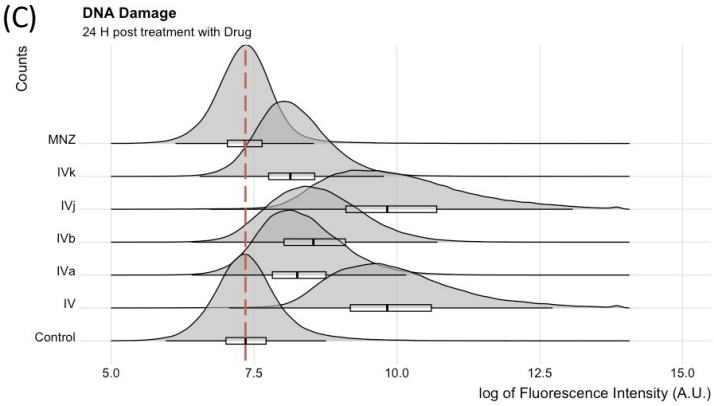
DNA Damage
24 H post treatment with Drug
Counts
MNZ
IVk
IVj
IVb
IVa
IV
Control
log of Fluorescence Intensity (A.U.)

(D)

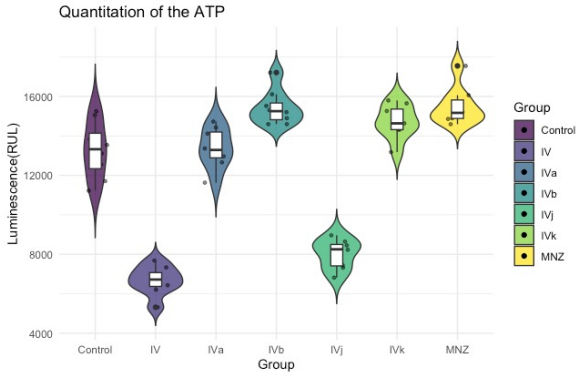
Quantitation of the ATP
Luminescence(RUL)
Group
Control
IV
IVa
IVb
IVj
IVk
MNZ

(E)

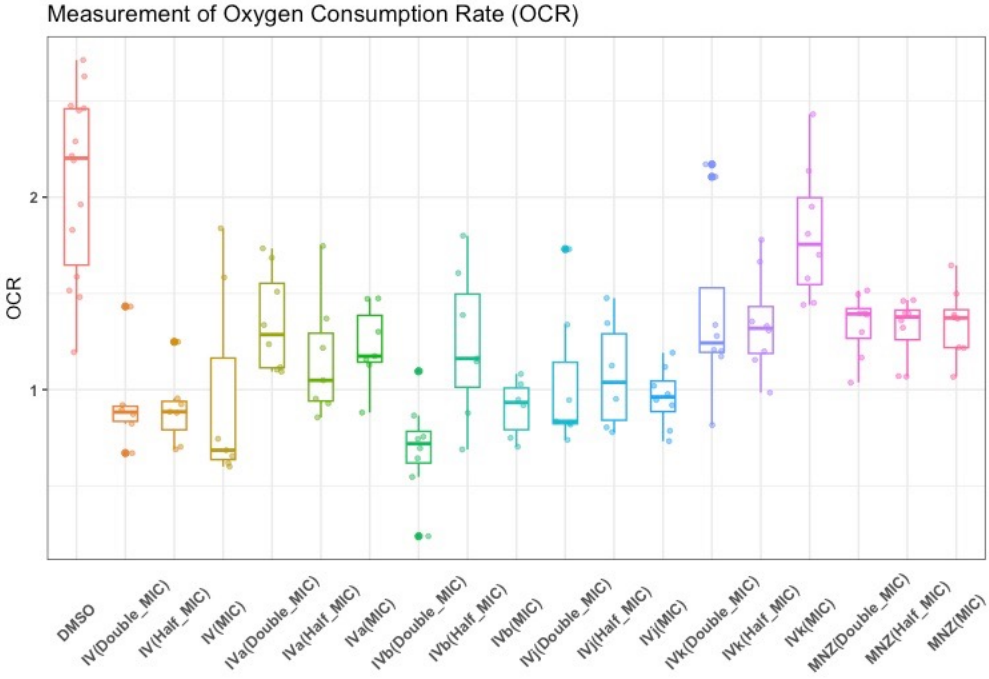
Measurement of Oxygen Consumption Rate (OCR)
OCR
DMSO
IV(Double_MIC)
IV(Half_MIC)
IV(MIC)
IVa(Double_MIC)
IVa(Half_MIC)
IVa(MIC)
IVb(Double_MIC)
IVb(Half_MIC)
IVb(MIC)
IVj(Double_MIC)
IVj(Half_MIC)
IVj(MIC)
IVk(Double_MIC)
IVk(Half_MIC)
IVk(MIC)
MNZ(Double_MIC)
MNZ(Half_MIC)
MNZ(MIC)

Fig. 6 Biophysical assays validating changes in the targeted pathway.

(A) The time-kill curves were obtained by measuring the bacterial growth inhibition using an initial inoculum of 10^5 CFU/ml at various time points up to 24 hours.

(B) Flow cytometry analysis was utilized to quantify the generation of reactive oxygen species (ROS), with fluorescence intensity plotted against counts. The presented data represents the compilation of three independent experiments.

(C) Flow cytometry analysis was performed on both control and drug-treated H. pylori cells following the TUNEL (Terminal deoxynucleotidyl transferase dUTP nick end labelling) assay protocol. The data is presented as a density plot of fluorescence intensity versus the cell counts. The presented data represents the compilation of three independent experiments.

(D) Changes in the ATP production rate and The presented data represent eight replicates of a single experiment.

(E) OCR of each sample (with 6 replicates) at 60 minutes was related to the basal OCR and compared with the same ratio obtained with the sole DMSO (as the untreated reference sample). Values are the means of the replicates ±SD.

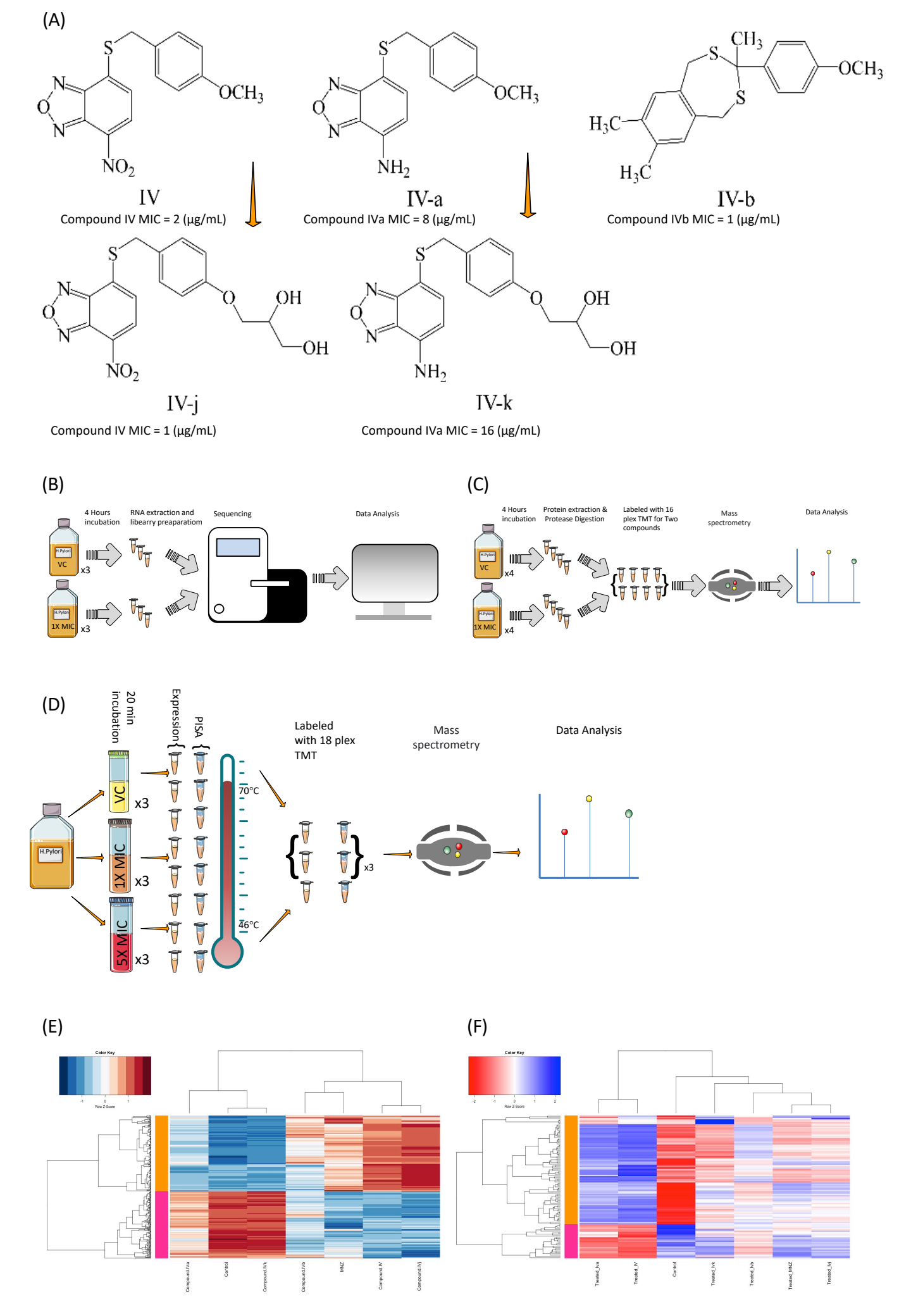
(A)
IV
Compound IV MIC = 2 (μg/mL)
IV-a
Compound IVa MIC = 8 (μg/mL)
IV-b
Compound IVb MIC = 1 (μg/mL)
IV-j
Compound IV MIC = 1 (μg/mL)
IV-k
Compound IVa MIC = 16 (μg/mL)
(B)
4 Hours incubation
RNA extraction and libearry preaparatiom
Sequencing
Data Analysis
VC
1X MIC
x3
(C)
4 Hours incubation
Protein extraction & Protease Digestion
Labeled with 16 plex TMT for Two compounds
Mass spectrometry
Data Analysis
VC
1X MIC
x4
(D)
20 min incubation
Expression
PISA
Labeled with 18 plex TMT
Mass spectrometry
Data Analysis
H.Pylori
VC
1X MIC
5X MIC
x3
70°C
46°C
(E)
Color Key
Row Z-Score
Compound IVa
Control
Compound IVk
Compound IVb
MNZ
Compound IV
Compound IVj
(F)
Color Key
Row Z-Score
Treated_Iva
Treated_IV
Control
Treated_Ivk
Treated_Ivb
Treated_MNZ
Treated_Ivj

Fig. S1 Compounds used in the assay and the study design.
(A) The compounds used in this assay were selected from a high-throughput screening that aimed to identify flavodoxin binders from a diverse chemical library of 10,000 compounds. Through several rounds of chemical variation and efficacy testing, a family of novel nitrobenzoxadiazol-based antimicrobials emerged, with compound IV as the lead compound. Compound IVj and IVk are more soluble derivatives of compound IV, and IVa is a derivative of compound IV with an amine functionality. The compounds bearing an amine functionality are narrow-spectrum antimicrobials that exhibit high specificity against H. pylori and potentially other gastric Helicobacter species but not enterohepatic Helicobacter species. The two compounds tested that contain a nitro functionality show extended-spectrum activity against Gram-positive bacteria, the Helicobacter genus, and C. jejuni. These extended-spectrum antimicrobials may have potential for novel therapies against Gram-positive bacteria, while the narrow-spectrum ones may be useful specifically against H. pylori.
(B) Transcriptomics Study Design for Drug Testing: Provide a description of the transcriptomics study design for drug testing.
(C) Proteomics Assay Study Design for Drug Testing: Provide a description of the proteomics assay study design for drug testing.
(D) Proteome Integral Solubility Alteration (PISA) Assay Study Design for Determination of Intracellular Targets: Provide a description of the Proteome Integral Solubility Alteration (PISA) assay study design for determining intracellular targets.
(E) The heatmap displays 771 differentially expressed genes, and hierarchical clustering is performed based on different compounds.
(F) The heatmap represents 113 differentially expressed proteins, and hierarchical clustering is conducted based on different compounds.

(A)

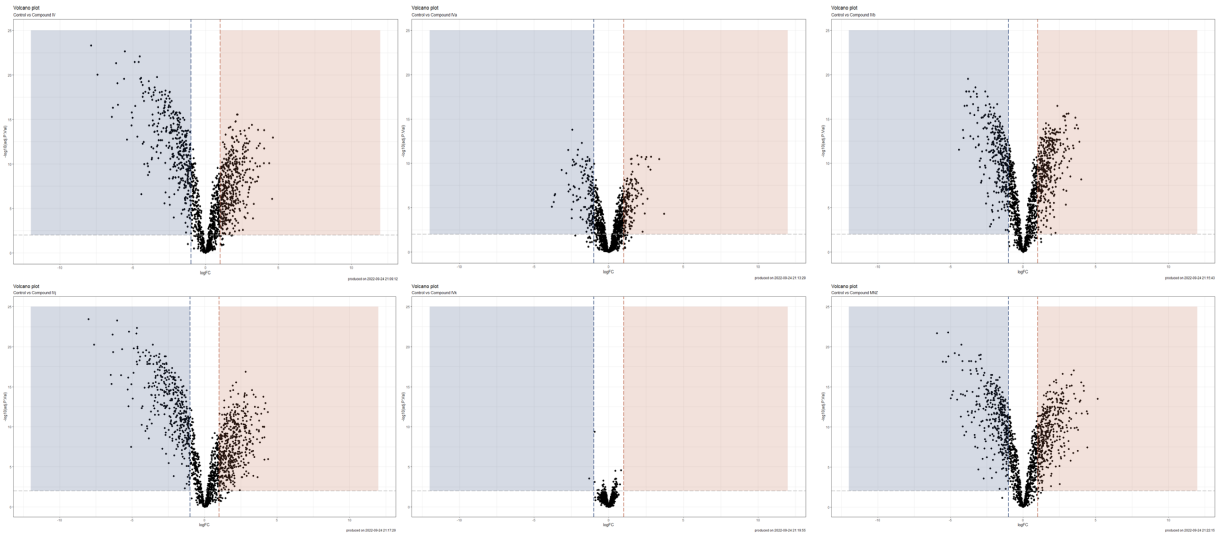

(B)

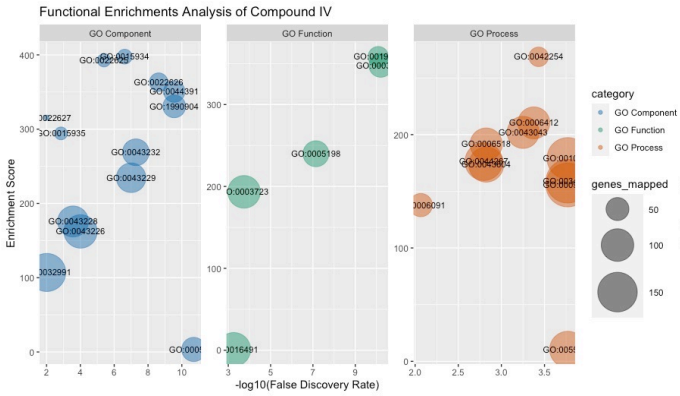
Functional Enrichments Analysis of Compound IV
GO Component
GO Function
GO Process
Enrichment Score
-log10(False Discovery Rate)
category
GO Component
GO Function
GO Process
genes_mapped
50
100
150

(C)

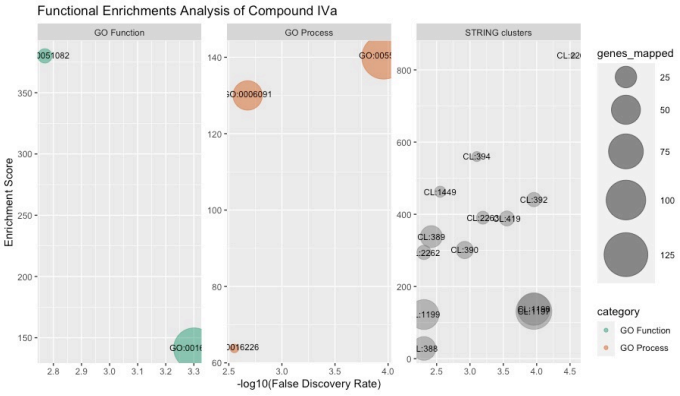
Functional Enrichments Analysis of Compound IVa
GO Function
GO Process
STRING clusters
Enrichment Score
-log10(False Discovery Rate)
genes_mapped
25
50
75
100
125
category
GO Function
GO Process

(D)

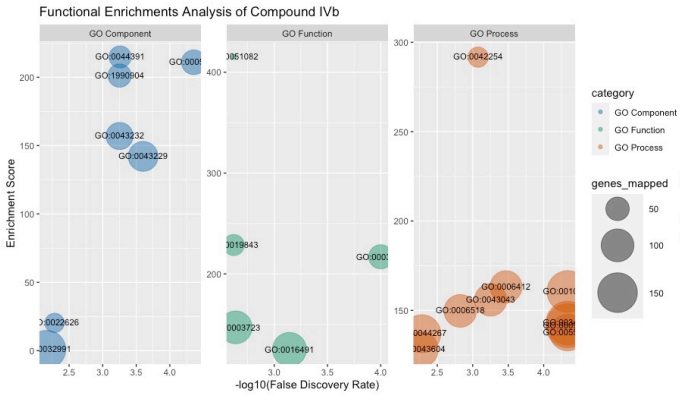
Functional Enrichments Analysis of Compound IVb
GO Component
GO Function
GO Process
Enrichment Score
-log10(False Discovery Rate)
category
GO Component
GO Function
GO Process
genes_mapped
50
100
150

(E)

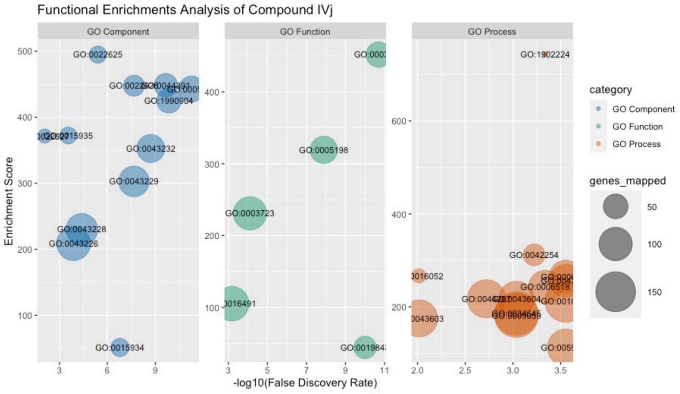
Functional Enrichments Analysis of Compound IVj
GO Component
GO Function
GO Process
Enrichment Score
-log10(False Discovery Rate)
category
GO Component
GO Function
GO Process
genes_mapped
50
100
150

(F)

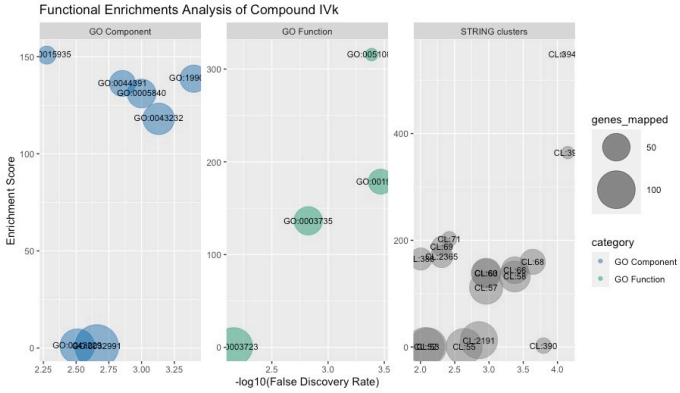
Functional Enrichments Analysis of Compound IVk
GO Component
GO Function
STRING clusters
Enrichment Score
-log10(False Discovery Rate)
genes_mapped
50
100
category
GO Component
GO Function

(G)

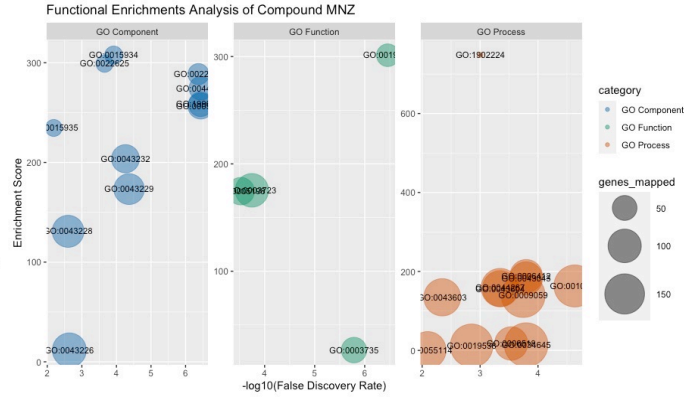
Functional Enrichments Analysis of Compound MNZ
GO Component
GO Function
GO Process
Enrichment Score
-log10(False Discovery Rate)
category
GO Component
GO Function
GO Process
genes_mapped
50
100
150

Fig. S2 **Gene ontology analysis of Compound IV and its derivatives**
(A) Volcano plot: Displays the differentially expressed genes identified from the transcriptomics assay.
(B) Distribution of gene ontology components associated with Compound IV: Shows the distribution of gene ontology terms associated with the biological processes, molecular functions, and cellular components influenced by Compound IV.
(C) Distribution of gene ontology components and String cluster associated with Compound IVa: Presents the distribution of gene ontology terms and String cluster analysis results associated with Compound IVa.
(D) Distribution of gene ontology components associated with Compound IVb: Illustrates the distribution of gene ontology terms associated with the biological processes, molecular functions, and cellular components influenced by Compound IVb.
(E) Distribution of gene ontology components associated with Compound IVj: Shows the distribution of gene ontology terms associated with the biological processes, molecular functions, and cellular components influenced by Compound IVj.
(F) Distribution of gene ontology components and String cluster associated with Compound IVk: Presents the distribution of gene ontology terms and String cluster analysis results associated with Compound IVk, which is a more soluble derivative of Compound IVa.
(G) Distribution of gene ontology components associated with Compound MNZ: Depicts the distribution of gene ontology terms associated with the biological processes, molecular functions, and cellular components influenced by Compound MNZ.

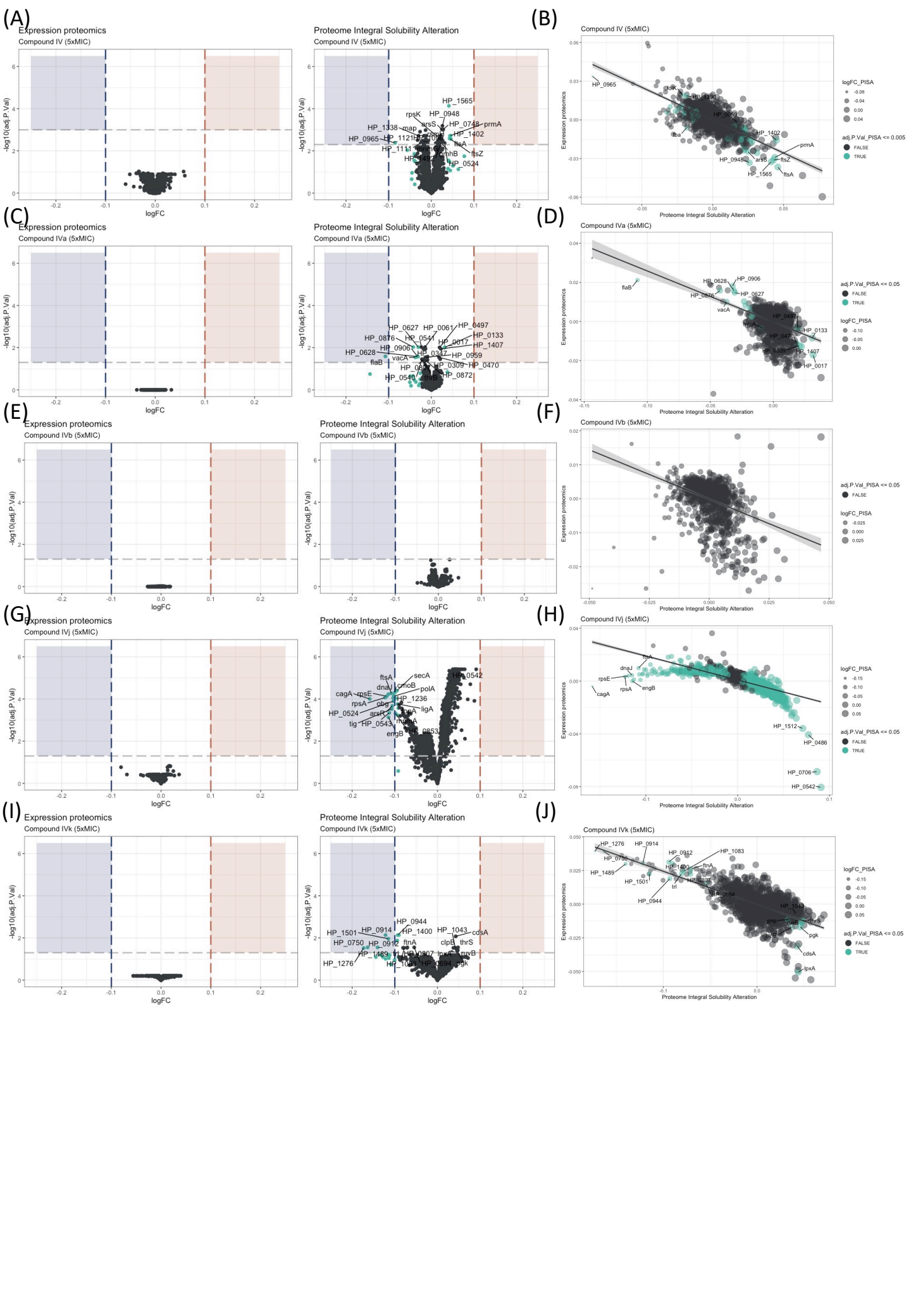
(A)
Expression proteomics
Compound IV (5xMIC)
Proteome Integral Solubility Alteration
Compound IV (5xMIC)
-log10(adj.P.Val)
logFC
(B)
Compound IV (5xMIC)
Expression proteomics
Proteome Integral Solubility Alteration
logFC_PISA
adj.P.Val_PISA <= 0.005
FALSE
TRUE
(C)
Expression proteomics
Compound IVa (5xMIC)
Proteome Integral Solubility Alteration
Compound IVa (5xMIC)
(D)
Compound IVa (5xMIC)
adj.P.Val_PISA <= 0.05
(E)
Expression proteomics
Compound IVb (5xMIC)
Proteome Integral Solubility Alteration
Compound IVb (5xMIC)
(F)
Compound IVb (5xMIC)
(G)
Expression proteomics
Compound IVj (5xMIC)
Proteome Integral Solubility Alteration
Compound IVj (5xMIC)
(H)
Compound IVj (5xMIC)
(I)
Expression proteomics
Compound IVk (5xMIC)
Proteome Integral Solubility Alteration
Compound IVk (5xMIC)
(J)
Compound IVk (5xMIC)

Fig. S3 **Proteome Integral Solubility Alteration coupled with expression proteomics (PISA-Express) analysis for different compounds at 5x of MIC.**

(A) Changes in expression proteomics data and Proteome Integral Solubility Alteration results in five times of MIC concentrations of Compound IV.

(B) Comparison of the expression proteomics data with Proteome Integral Solubility Alteration demonstrates significant alterations (teal color) in protein solubility for Compound IV.

(C) Changes in expression proteomics data and Proteome Integral Solubility Alteration results in five times of MIC concentrations of Compound IVa.

(D) Comparison of the expression proteomics data with Proteome Integral Solubility Alteration demonstrates significant alterations (teal color) in protein solubility for Compound IVa.

(E) Compound IVb does not revile any Changes in expression proteomics data and Proteome Integral Solubility Alteration results in five times of MIC concentrations of Compound IVb.

(F) Comparison of the expression proteomics data and Proteome Integral Solubility Alteration results with five times of MIC concentrations of Compound IVb showing a negative correlation but does not revile any significant changes.

(G) Changes in expression proteomics data and Proteome Integral Solubility Alteration results in five times of MIC concentrations of Compound IVj.

(H) Comparison of the expression proteomics data with Proteome Integral Solubility Alteration demonstrates significant alterations (teal color) in protein solubility for Compound IVj.

(I) Changes in expression proteomics data and Proteome Integral Solubility Alteration results in five times of MIC concentrations of Compound IVk.

(J) Comparison of the expression proteomics data with Proteome Integral Solubility Alteration demonstrates significant alterations (teal color) in protein solubility for Compound IVk.

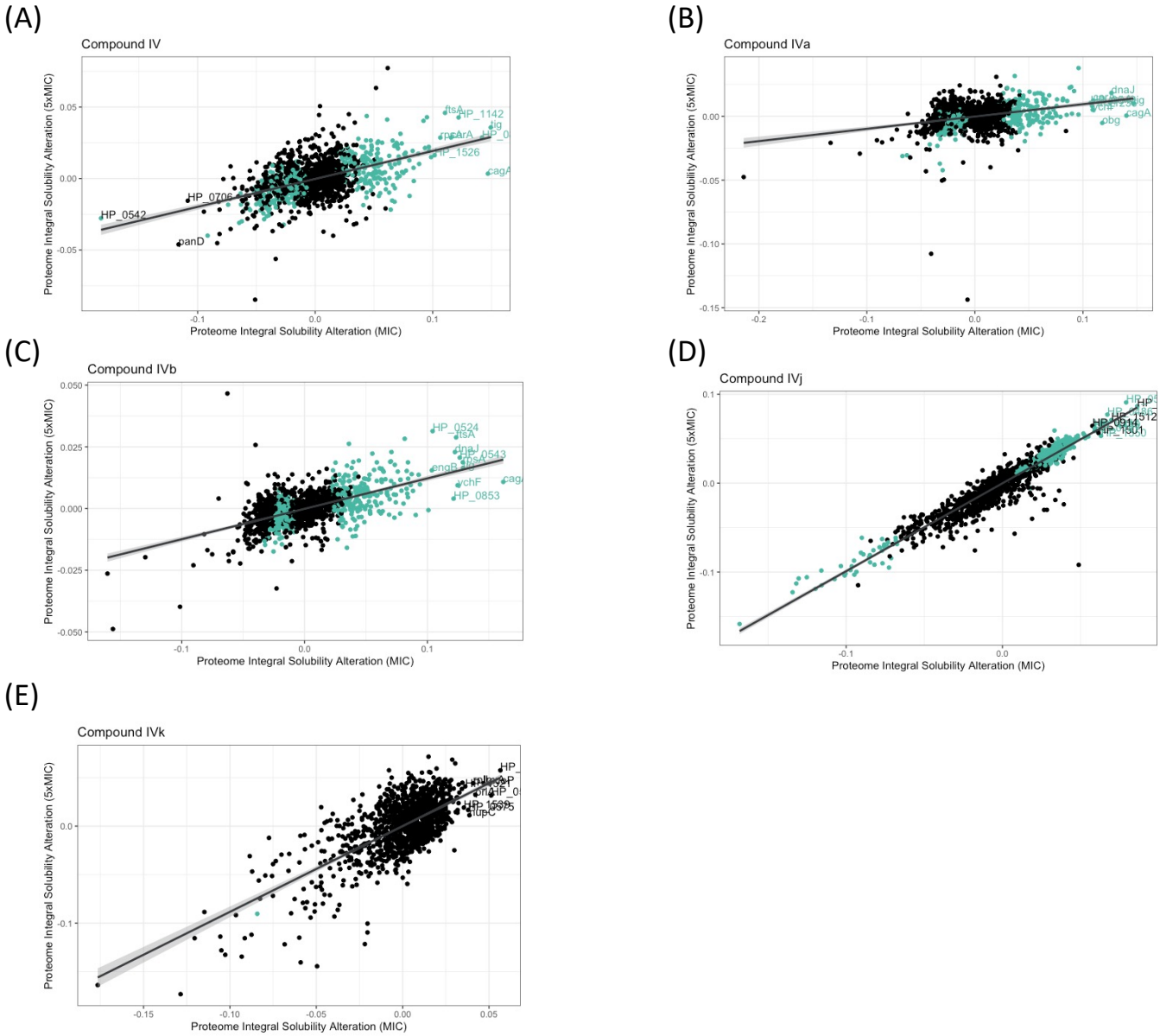
(A)
Compound IV
Proteome Integral Solubility Alteration (5xMIC)
Proteome Integral Solubility Alteration (MIC)
HP_0542
HP_0706
panD
ftsA
HP_1142
lig
HP_1526
cagA
(B)
Compound IVa
Proteome Integral Solubility Alteration (5xMIC)
Proteome Integral Solubility Alteration (MIC)
dnaJ
cagA
obg
(C)
Compound IVb
Proteome Integral Solubility Alteration (5xMIC)
Proteome Integral Solubility Alteration (MIC)
HP_0524
ftsA
dnaJ
HP_0543
engB
vchF
HP_0853
(D)
Compound IVj
Proteome Integral Solubility Alteration (5xMIC)
Proteome Integral Solubility Alteration (MIC)
HP_1512
HP_0914
HP_1501
(E)
Compound IVk
Proteome Integral Solubility Alteration (5xMIC)
Proteome Integral Solubility Alteration (MIC)
HP_1575
lupC

Fig. S4 **Concentration-dependent changes in Proteome Integral Solubility Alteration**

(A) Concentration-dependent targets for Compound IV: Shows the targets that exhibit a concentration-dependent response to Compound IV, represented by the teal color.
(B) Concentration-dependent targets for Compound IVa: Shows the targets that exhibit a concentration-dependent response to Compound IVa, represented by the teal color.
(C) Concentration-dependent targets for Compound IVb: Shows the targets that exhibit a concentration-dependent response to Compound IVb, represented by the teal color.
(D) Concentration-dependent targets for Compound IVj: Shows the targets that exhibit a concentration-dependent response to Compound IVj, represented by the teal color.
(D) We have not detected any significant concentration-dependent targets for Compound IVk.

(A)

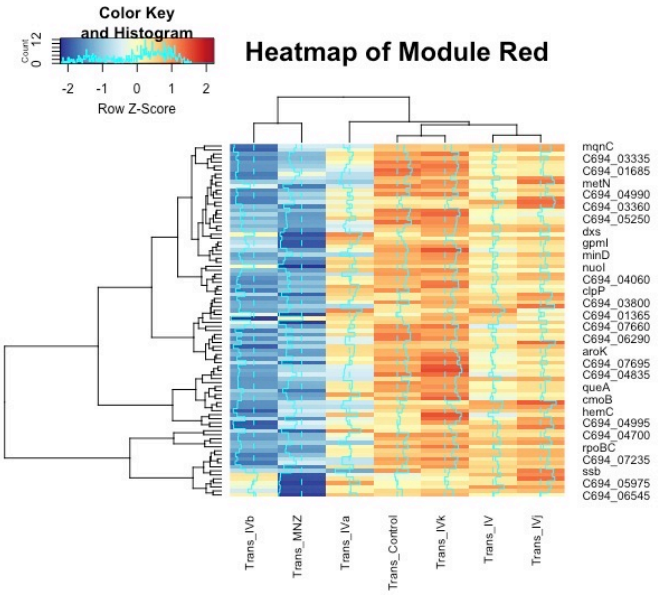

(B)

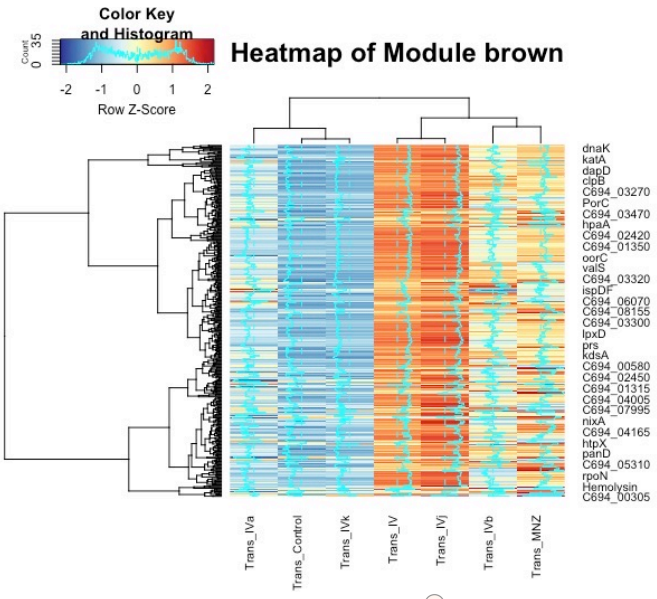

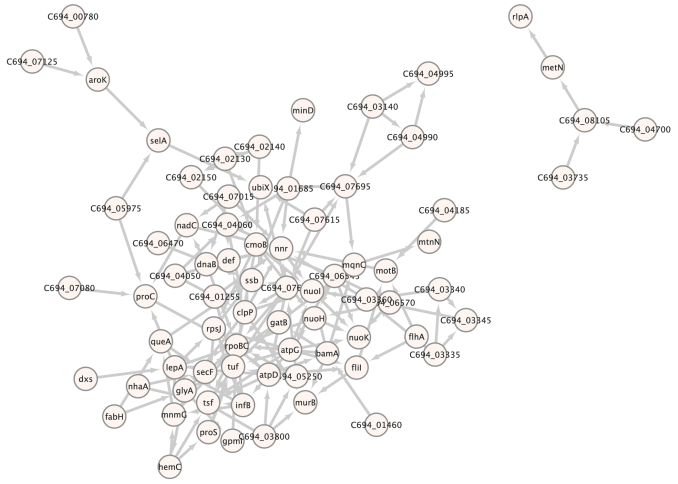

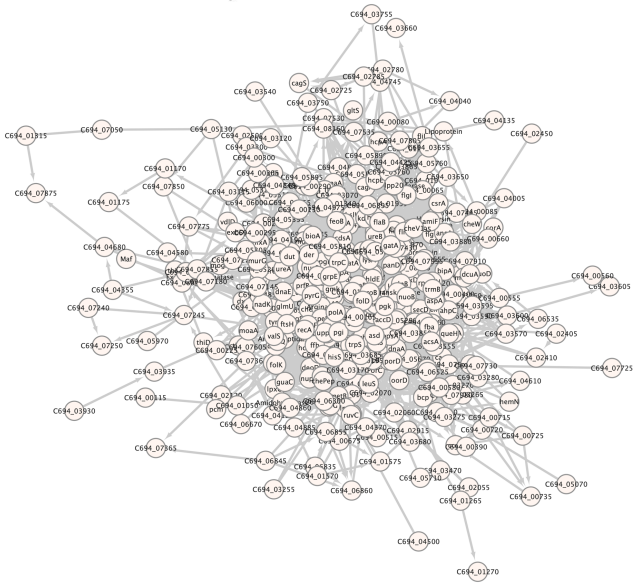

Term ID	Term description	Strength	FDR
GO:0110165	Cellular anatomical entity	0.11	0.0084
GO:0016020	Membrane	0.25	0.0118
KW-1278	Translocase	0.99	0.0076

Term ID	Term description	Strength	FDR
GO:0044281	Small molecule metabolic process	0.2	0.0060
GO:0055114	Oxidation-reduction process	0.29	0.0060
GO:0019752	Carboxylic acid metabolic process	0.25	0.0121
GO:0003824	Catalytic activity	0.11	8.06e-05
GO:0043167	Ion binding	0.14	0.0032
GO:0016491	Oxidoreductase activity	0.28	0.0131
GO:0036094	Small molecule binding	0.17	0.0156
GO:0005737	Cytoplasm	0.13	0.00029
GO:0005622	Intracellular	0.11	0.00088
GO:0110165	Cellular anatomical entity	0.06	0.00088
GO:0005829	Cytosol	0.14	0.0429
CL:1197	Carbon metabolism, and fatty acid metabolic process	0.36	0.00068
CL:1198	Carbon metabolism, and fatty acid metabolic process	0.4	0.00068
CL:1199	Carbon metabolism, and fatty acid synthase activity	0.4	0.0026
CL:1201	Pyruvate metabolism, and Citrate cycle (TCA cycle)	0.47	0.0330
heo01100	Metabolic pathways	0.2	2.45e-05
heo01110	Biosynthesis of secondary metabolites	0.26	0.00047
heo01120	Microbial metabolism in diverse environments	0.31	0.0029
heo01200	Carbon metabolism	0.38	0.0029
heo02020	Two-component system	0.42	0.0101
heo00020	Citrate cycle (TCA cycle)	0.49	0.0425
heo01230	Biosynthesis of amino acids	0.28	0.0457

Fig. S5 Gene expression heatmap and correlation of different compounds across modules from the WGCNA analysis.
(A) Gene expression heatmap and correlation in module "red": This figure shows the gene expression patterns of Compound IV and its derivatives, along with their correlation in the "red" module. It also depicts the protein-protein coexpression network of the genes in this module and the associated gene ontology.
(B) Gene expression heatmap and correlation in module "brown": This figure shows the gene expression patterns of Compound IV and its derivatives, along with their correlation in the "brown" module. It also illustrates the protein-protein coexpression network of the genes in this module and the associated gene ontology.

(A)

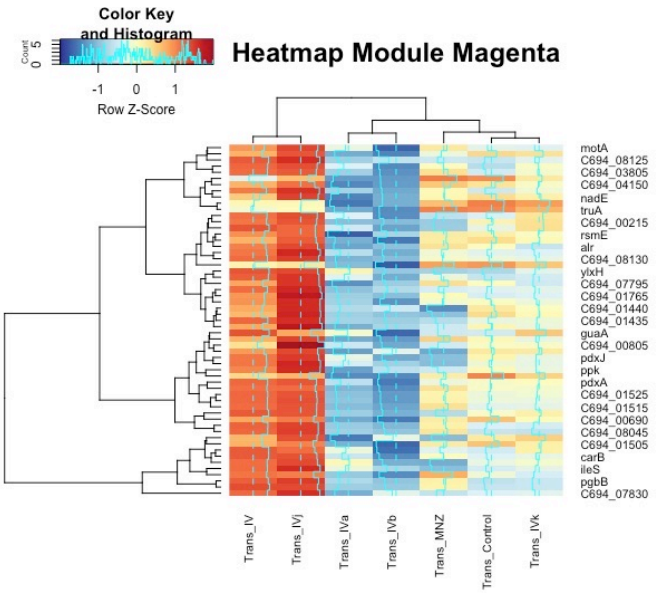

(B)

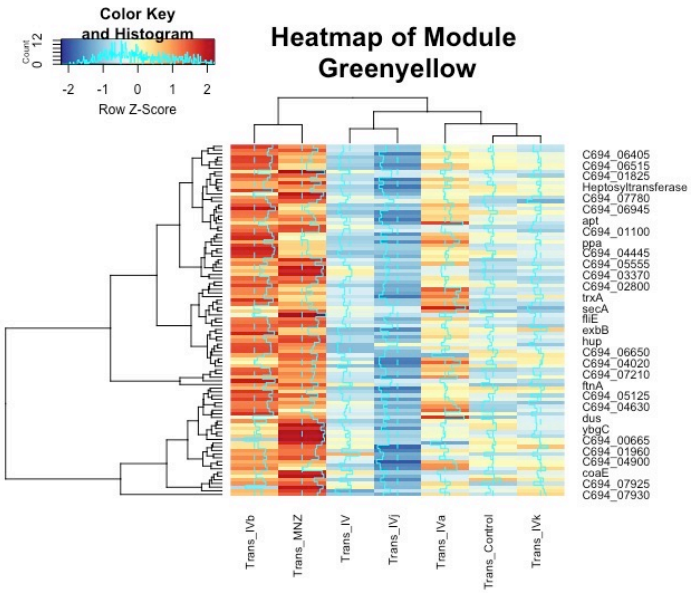

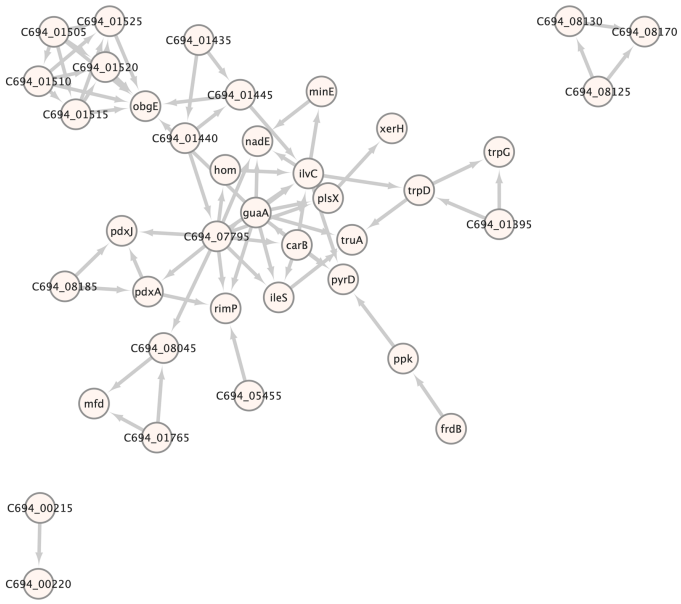

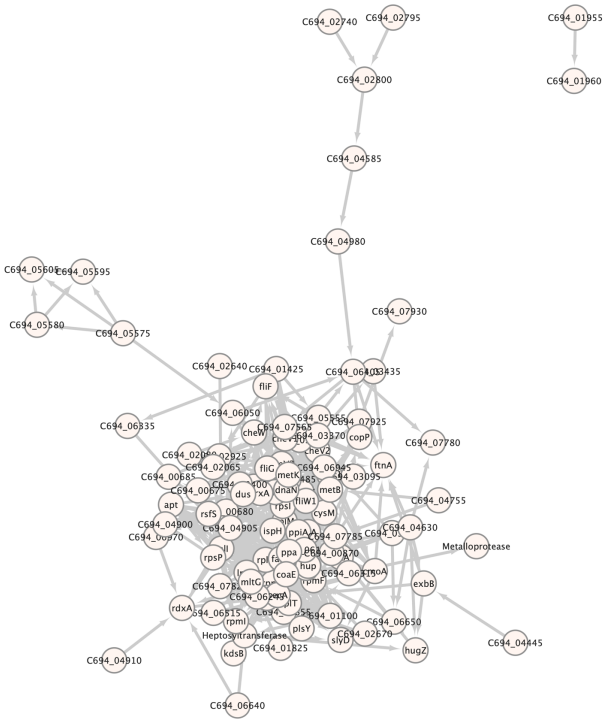

Term ID	Term description	Strength	FDR
CL:2616	Dipeptide transmembrane transporter activity, and Oligopeptide/dipeptide ABC transporter, C-terminal	1.45	0.0033

Term ID	Term description	Strength	FDR
GO:0006935	Chemotaxis	0.99	0.00013
GO:0040011	Locomotion	0.78	0.00031
GO:0007165	Signal transduction	0.88	0.0020
GO:0042221	Response to chemical	0.68	0.0020
GO:0007154	Cell communication	0.69	0.0108
CL:1948	Taxis	1.1	9.53e-05
CL:1869	Locomotion, and cell projection organization	0.58	0.0018
CL:1870	Locomotion, and cell projection organization	0.59	0.0018
CL:1871	Locomotion, and cell projection organization	0.61	0.0018
CL:1951	CheW-like domain, and Transducer	1.14	0.0130
heo02030	Bacterial chemotaxis	0.98	4.04e-05
SM00260	Two component signalling adaptor domain	1.14	0.0109
SM00283	Methyl-accepting chemotaxis-like domains (chemotaxis sensory transducer).	1.14	0.0245
SM00448	cheY-homologous receiver domain	0.84	0.0327

Fig. S6 Gene expression heatmap and correlation of different compounds across modules from the WGCNA analysis.

(A) Gene expression heatmap and correlation in module “magents": This figure shows the gene expression patterns of Compound IV and its derivatives, along with their correlation in the " magents " module. It also depicts the protein-protein coexpression network of the genes in this module and the associated gene ontology.

(B) Gene expression heatmap and correlation in module “Greenyellow": This figure shows the gene expression patterns of Compound IV and its derivatives, along with their correlation in the " Greenyellow " module. It also illustrates the protein-protein coexpression network of the genes in this module and the associated gene ontology.

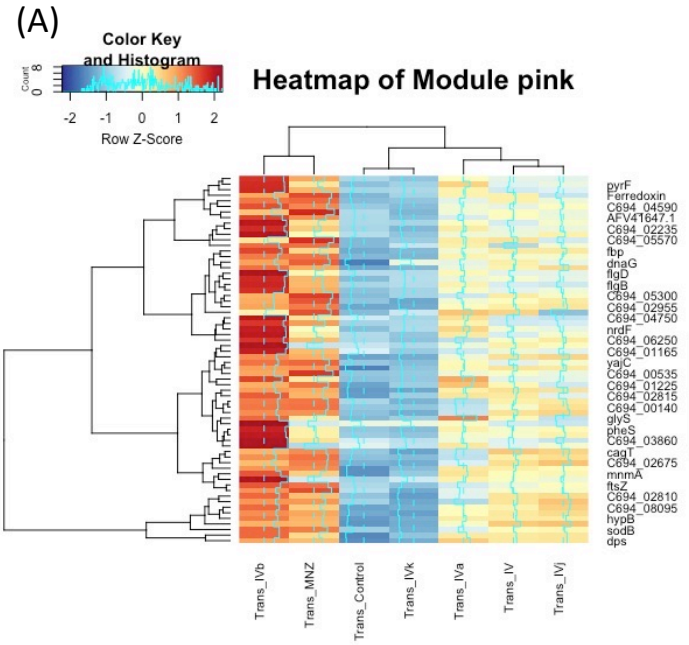

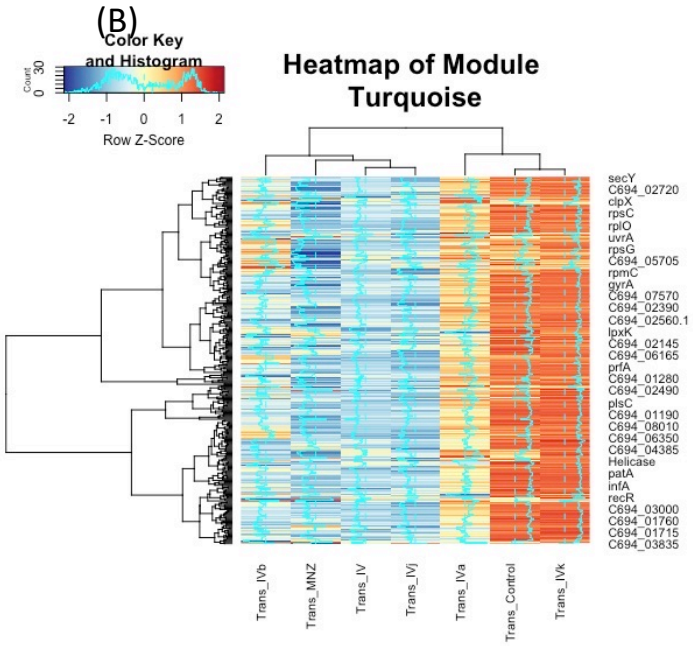

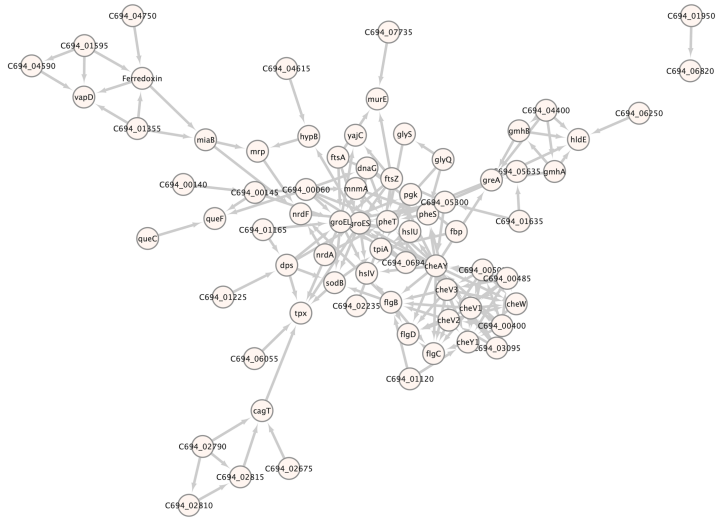

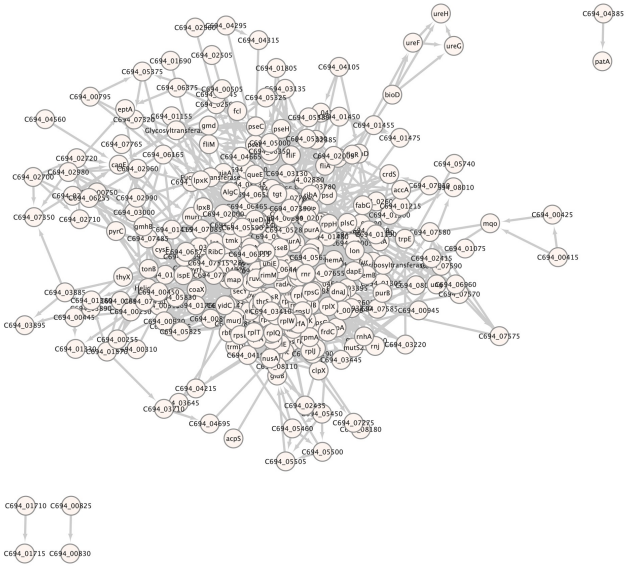

Term ID	Term description	Strength	FDR
GO:0006935	Chemotaxis	1.04	0.00037
GO:0007165	Signal transduction	1.01	0.00037
GO:0040011	Locomotion	0.84	0.00037
GO:0042221	Response to chemical	0.75	0.0012
CL:1948	Taxis	1.23	5.89e-06
CL:1871	Locomotion, and cell projection organization	0.67	0.0019
CL:1951	CheW-like domain, and Transducer	1.27	0.0057
CL:388	Mixed, incl. protein folding, and detoxification	0.68	0.0293
CL:1097	ADP-L-glycero-beta-D-manno-heptose metabolic process, and GmhA/DiaA	1.17	0.0299
CL:389	Mixed, incl. protein folding, and detoxification	0.7	0.0375
heo02030	Bacterial chemotaxis	1.02	0.00015
heo02020	Two-component system	0.72	0.0064
PF01584	CheW-like domain	1.27	0.0234
IPR002545	CheW-like domain	1.27	0.0369
IPR036061	CheW-like domain superfamily	1.27	0.0369
SM00260	Two component signalling adaptor domain	1.27	0.0028
SM00283	Methyl-accepting chemotaxis-like domains (chemotaxis sensory transducer).	1.27	0.0082
SM00448	cheY-homologous receiver domain	0.97	0.0090

Term ID	Term description	Strength	FDR
GO:0010467	Gene expression	0.32	6.00e-05
GO:0009059	Macromolecule biosynthetic process	0.28	9.53e-05
GO:0034645	Cellular macromolecule biosynthetic process	0.28	9.53e-05
GO:0044238	Primary metabolic process	0.14	9.53e-05
GO:0044249	Cellular biosynthetic process	0.19	9.53e-05
GO:1901576	Organic substance biosynthetic process	0.19	9.53e-05
GO:0071704	Organic substance metabolic process	0.12	0.00010
GO:0043170	Macromolecule metabolic process	0.17	0.00014
GO:0044271	Cellular nitrogen compound biosynthetic process	0.23	0.00022
GO:0006412	Translation	0.35	0.00054
GO:0043604	Amide biosynthetic process	0.32	0.00061
GO:0008152	Metabolic process	0.1	0.00069
GO:0044260	Cellular macromolecule metabolic process	0.18	0.00069
GO:0006807	Nitrogen compound metabolic process	0.13	0.00070
GO:0034641	Cellular nitrogen compound metabolic process	0.16	0.00070
GO:0044237	Cellular metabolic process	0.11	0.00070
GO:0019538	Protein metabolic process	0.25	0.0014
GO:0044267	Cellular protein metabolic process	0.28	0.0016
GO:0009987	Cellular process	0.07	0.0024

Fig. S7 Gene expression heatmap and correlation of different compounds across modules from the WGCNA analysis.

(A) Gene expression heatmap and correlation in module “pink": This figure shows the gene expression patterns of Compound IV and its derivatives, along with their correlation in the "pink" module. It also depicts the protein-protein coexpression network of the genes in this module and the associated gene ontology.

(B) Gene expression heatmap and correlation in module “turquoise": This figure shows the gene expression patterns of Compound IV and its derivatives, along with their correlation in the " turquoise " module. It also illustrates the protein-protein coexpression network of the genes in this module and the associated gene ontology.

(A)

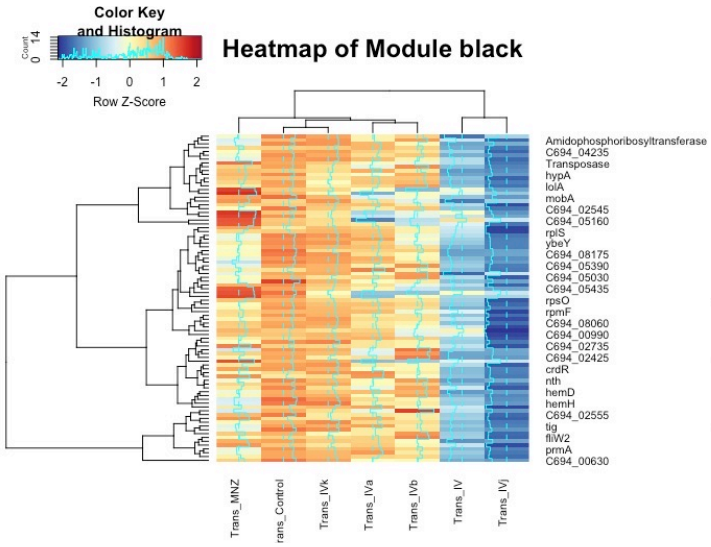

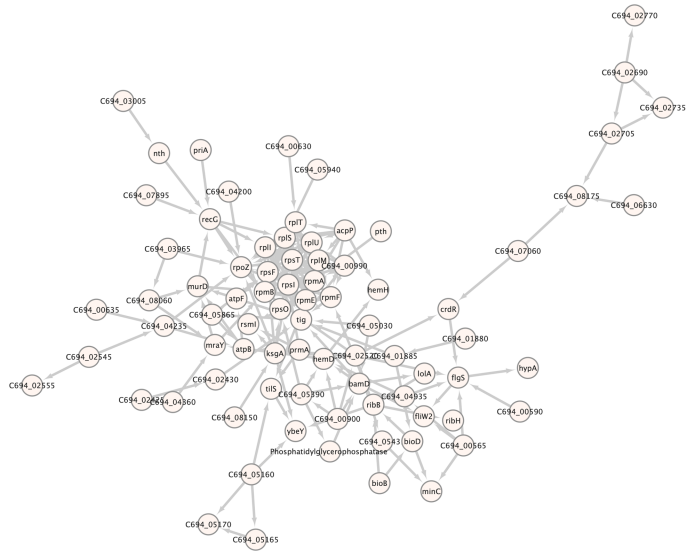

(B)

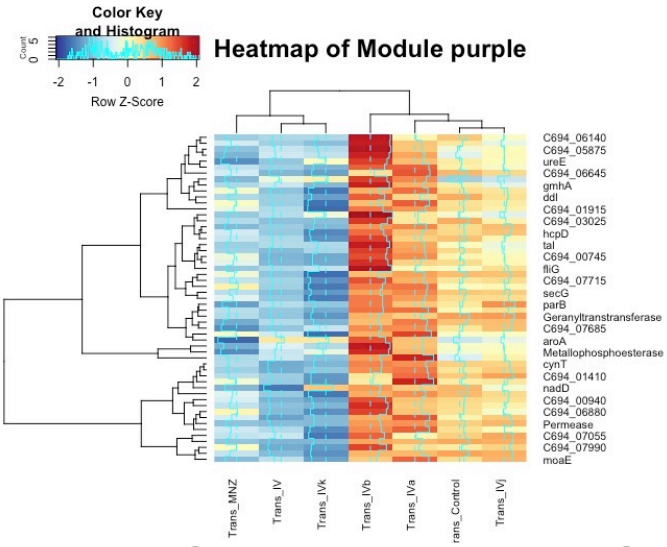

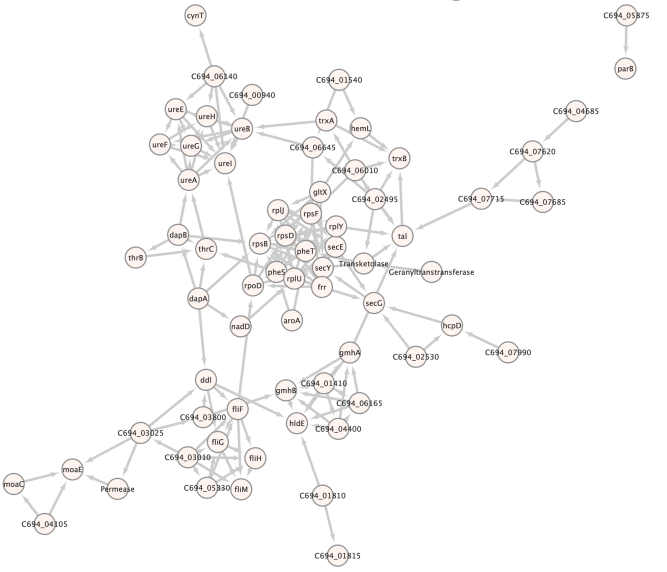

Term ID	Term description	Strength	FDR
GO:0043170	Macromolecule metabolic process	0.25	0.0132
GO:0044260	Cellular macromolecule metabolic process	0.27	0.0330
GO:0003735	Structural constituent of ribosome	0.61	0.0396
GO:0032991	Protein-containing complex	0.44	0.0018
GO:0005840	Ribosome	0.59	0.0044
GO:0043229	Intracellular organelle	0.5	0.0044
GO:0043232	Intracellular non-membrane-bounded organelle	0.54	0.0044
GO:1990904	Ribonucleoprotein complex	0.57	0.0100
GO:0044391	Ribosomal subunit	0.58	0.0145
GO:0022626	Cytosolic ribosome	0.59	0.0321
CL:55	Translation	0.47	0.0203
CL:57	Ribosome, and transcription, DNA-templated	0.52	0.0203
CL:58	Ribosome	0.56	0.0203
CL:63	Ribosome	0.6	0.0203
CL:66	Ribosome	0.63	0.0203
CL:51	Translation, and RNA methylation	0.39	0.0354
CL:118	Large ribosomal subunit	0.79	0.0369
CL:68	Ribosome	0.56	0.0498
heo03010	Ribosome	0.61	0.0042
KW-0689	Ribosomal protein	0.61	0.0096

Term ID	Term description	Strength	FDR
GO:0009405	Pathogenesis	0.95	0.0201
GO:0044419	Interspecies interaction between organisms	0.64	0.0299
GO:0003774	Motor activity	1.15	0.0254
GO:0016151	Nickel cation binding	1.05	0.0312
GO:0110165	Cellular anatomical entity	0.12	0.0017
GO:0005622	Intracellular	0.18	0.0178
GO:0005737	Cytoplasm	0.18	0.0308
CL:2821	Nickel insertion, and urease activity	1.27	0.0037
CL:1877	Motor activity, and Bacterial flagellum protein export	0.97	0.0290
CL:2796	Nickel cation binding, and protein maturation	0.82	0.0311
KW-0843	Virulence	1.0	0.0061
KW-0996	Nickel insertion	1.27	0.0371

Fig. S8 Gene expression heatmap and correlation of different compounds across modules from the WGCNA analysis.

(A) Gene expression heatmap and correlation in module “black": This figure shows the gene expression patterns of Compound IV and its derivatives, along with their correlation in the " black " module. It also depicts the protein-protein coexpression network of the genes in this module and the associated gene ontology.

(B) Gene expression heatmap and correlation in module “purple": This figure shows the gene expression patterns of Compound IV and its derivatives, along with their correlation in the " purple" module. It also illustrates the protein-protein coexpression network of the genes in this module and the associated gene ontology.

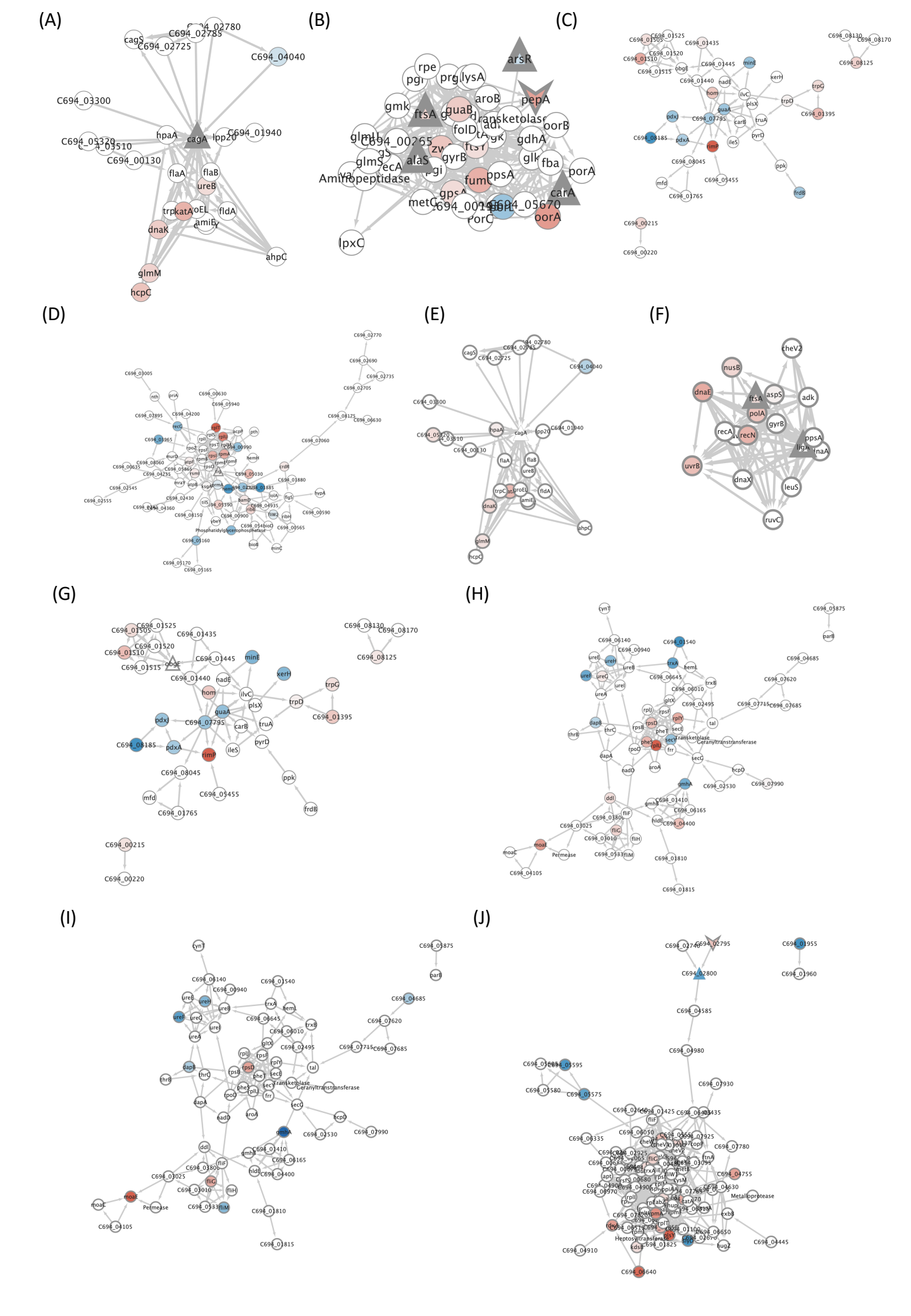
(A)
C694_02780
C694_02785
cagS
C694_02725
C694_04040
C694_03300
C694_03320
C694_03510
hpaA
cagA
lpp20
C694_01940
C694_00130
flaA
flaB
ureB
trpkatA
oEL
fldA
amiE
dnaK
ahpC
glmM
hcpC
(B)
arsR
rpe
prg
lysA
pepA
gmk
ftsA
guaB
aroB
transketolase
oorB
folD
gdhA
glmU
C694_00265
ftsI
gyrB
glmS
alaS
ecA
pgi
glk
fba
porA
Aminopeptidase
fumC
ppsA
carA
metC
C694_00190
C694_05670
PorC
oorA
lpxC
(C)
C694_01525
C694_01505
C694_01435
C694_01520
C694_01510
C694_01445
minE
C694_01515
obgE
C694_01440
nadE
kerH
hom
ilvC
trpC
plsX
trpD
C694_01395
pdxJ
C694_07795
guaA
carB
truA
C694_08185
pdxA
ileS
pyrD
rimP
C694_08045
ppk
C694_05455
mfd
C694_01765
frdB
C694_00215
C694_00220
C694_08130
C694_08170
C694_08125
(D)
C694_02770
C694_02690
C694_02735
C694_02705
C694_03005
C694_00630
C694_05940
C694_08125
C694_06630
C694_02895
C694_04200
C694_02060
C694_03965
C694_08060
C694_00633
C694_05865
C694_04254
C694_05030
C694_01880
C694_02545
C694_02555
C694_02430
C694_04360
C694_08150
C694_04935
C694_00590
C694_00900
C694_00565
C694_01160
C694_05170
C694_05165
(E)
C694_02780
C694_02785
cagS
C694_02725
C694_04040
C694_03800
C694_05020
C694_03510
hpaA
cagA
lpp20
C694_01940
C694_00130
flaA
flaB
ureB
trpC
oEL
fldA
amiE
dnaK
ahpC
glmM
hcpC
(F)
cheV2
nusB
dnaE
ftsA
aspS
adk
polA
gyrB
recA
recN
ppsA
uvrB
dnaX
leuS
ruvC
(G)
C694_01525
C694_01505
C694_01435
C694_01520
C694_01510
C694_01445
minE
C694_01515
obgE
C694_01440
nadE
xerH
hom
ilvC
trpC
plsX
trpD
C694_01395
pdxJ
C694_07795
guaA
carB
truA
C694_08185
pdxA
ileS
pyrD
rimP
C694_08045
ppk
C694_05455
mfd
C694_01765
frdB
C694_00215
C694_00220
C694_08130
C694_08170
C694_08125
(H)
cynT
C694_03875
parB
C694_06140
C694_00940
C694_01540
C694_04685
ureE
ureH
ureB
trxA
hemL
ureF
ureG
ureI
C694_06645
trxB
C694_07620
ureA
C694_06010
gltX
C694_02495
C694_07715
C694_07685
rplU
rpsF
rplY
dapB
rpsB
rpsD
tal
thrB
thrC
pheT
secE
Transketolase
Geranyltranstransferase
phes
secY
rplU
frr
rpoD
dapA
secG
nadD
aroA
hcpD
gmhA
C694_02530
C694_07990
ddl
C694_01410
gmhB
C694_06165
fliF
C694_03800
hldE
C694_04400
C694_03025
fliG
C694_03010
fliH
moaE
Permease
C694_05335
fliM
C694_01810
moaC
C694_04105
C694_01815
(I)
cynT
C694_03875
parB
C694_06140
C694_00940
C694_01540
C694_04685
ureE
ureH
ureB
trxA
hemL
ureF
ureG
ureI
C694_06645
trxB
C694_07620
ureA
C694_06010
gltX
C694_02495
C694_07715
C694_07685
rplU
rpsF
rplY
dapB
rpsB
rpsD
tal
thrB
thrC
pheT
secE
Transketolase
Geranyltranstransferase
phes
secY
rplU
frr
rpoD
dapA
secG
nadD
aroA
hcpD
gmhA
C694_02530
C694_07990
ddl
C694_01410
gmhB
C694_06165
fliF
C694_03800
hldE
C694_04400
C694_03025
fliG
C694_03010
fliH
moaE
Permease
C694_05335
fliM
C694_01810
moaC
C694_04105
C694_01815
(J)
C694_02746
C694_02795
C694_01955
C694_02800
C694_01960
C694_03585
C694_04980
C694_05605
C694_05595
C694_05580
C694_05575
C694_07930
C694_06260
C694_01425
C694_06240
C694_01435
fliF
C694_06335
C694_05050
C694_05365
C694_07925
C694_07780
C694_06680
C694_02925
C694_03095
C694_04755
C694_04630
C694_06970
C694_04905
C694_04490
Metalloprotease
C694_06915
exbB
C694_06650
C694_06570
C694_04445
C694_04910
C694_06640

Fig. S9 Associations between different modules and specific targets for Compound IV and its derivatives.
(A-B) First neighbors of the target proteins CagA and FtsA from the "brown" module associated with Compound IV. (C) Module "magenta" associated with Compound IV. (D) Module "black" associated with Compound IV, with Tig as a target. (E-F) First neighbors of the target proteins CagA and FtsA from the "brown" module associated with Compound IVa. (G) Module "magenta" associated with Compound IVa, with ObgE as a target. (H) Module "purple" associated with Compound IVa. (I) Module "purple" associated with Compound IVb. (J) Module "greenyellow" associated with Compound IVb, with two uncharacterized proteins as targets.

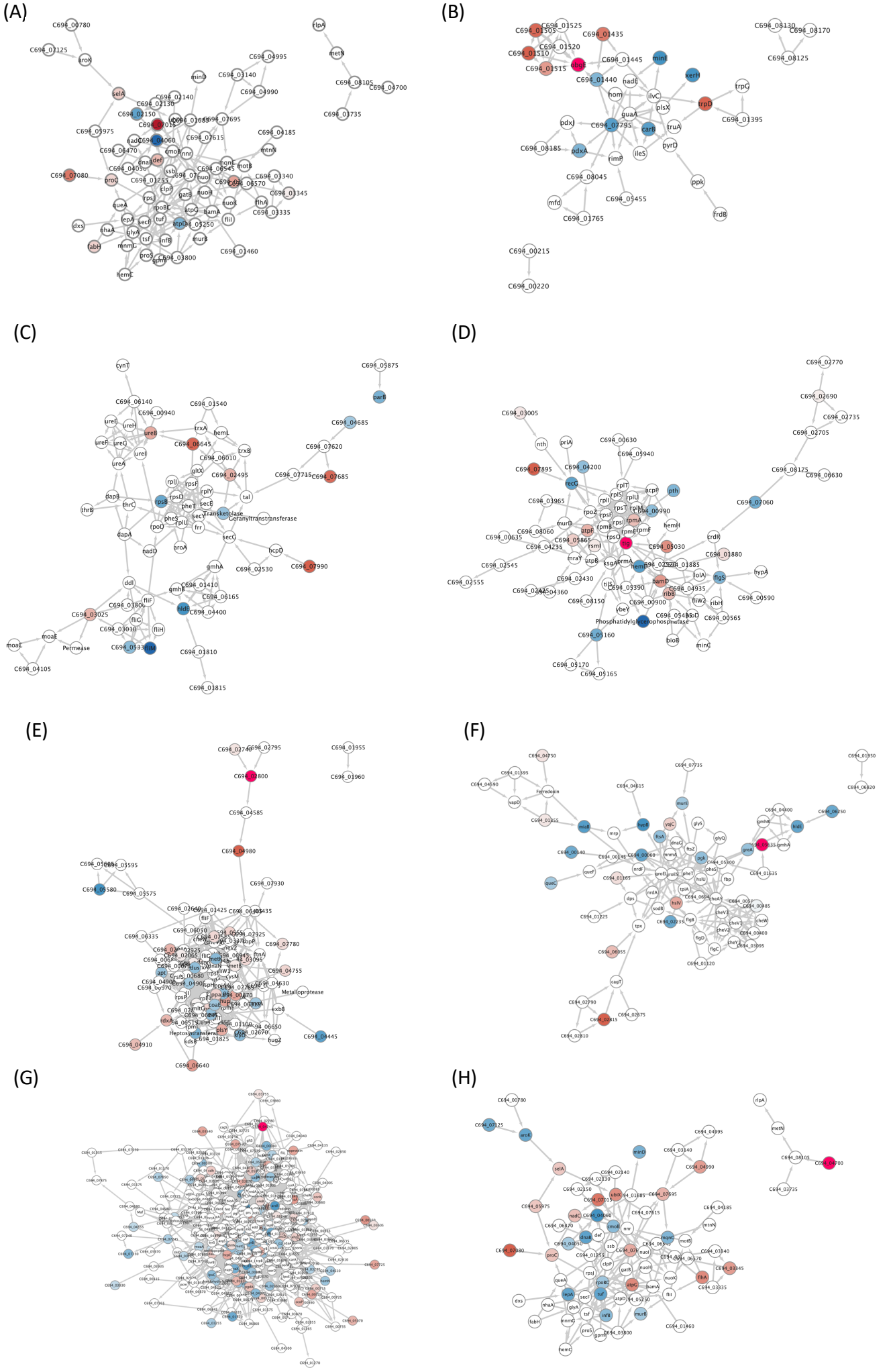
(A)
(B)
(C)
(D)
(E)
(F)
(G)
(H)

Fig. S10 Associations between different modules and specific targets for Compound IV and its derivatives.
(A) Module "red" associated with Compound IVb. (B) Module "magenta" associated with Compound IVb, with ObgE as a target. (C) Module "purple" associated with Compound IVj. (D) Module "black" associated with Compound IVj, with Tig as a target. (E) Module "greenyellow" associated with Compound IVj, with a hypothetical protein as a target. (F) Module "pink" associated with Compound IVk, with a hypothetical protein as a target. (G) Module "brown" associated with Compound IVk, with a hypothetical protein as a target. (H) Module "red" associated with Compound IVk, with a hypothetical protein as a target.

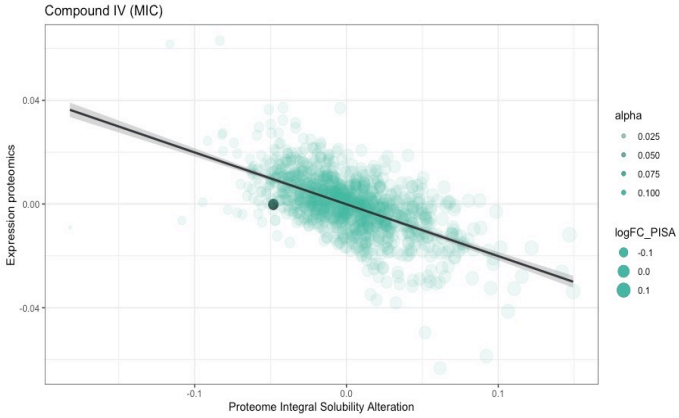
Compound IV (MIC)
Expression proteomics
Proteome Integral Solubility Alteration
alpha
0.025
0.050
0.075
0.100
logFC_PISA
-0.1
0.0
0.1

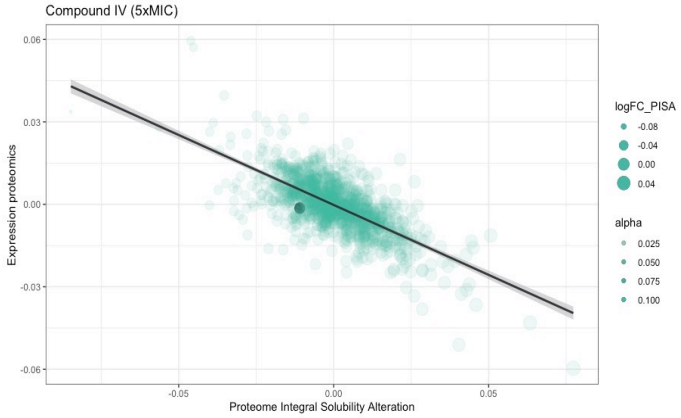
Compound IV (5xMIC)
Expression proteomics
Proteome Integral Solubility Alteration
logFC_PISA
-0.08
-0.04
0.00
0.04
alpha
0.025
0.050
0.075
0.100

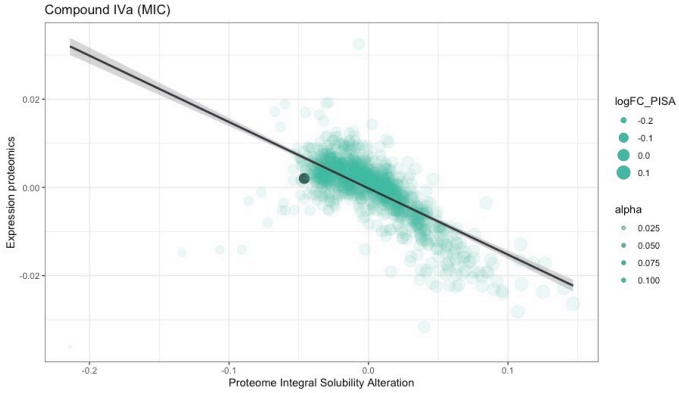
Compound IVa (MIC)
Expression proteomics
Proteome Integral Solubility Alteration
logFC_PISA
-0.2
-0.1
0.0
0.1
alpha
0.025
0.050
0.075
0.100

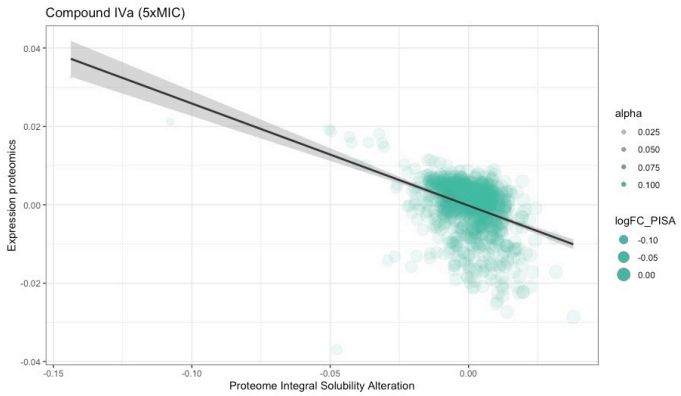
Compound IVa (5xMIC)
Expression proteomics
Proteome Integral Solubility Alteration
alpha
0.025
0.050
0.075
0.100
logFC_PISA
-0.10
-0.05
0.00

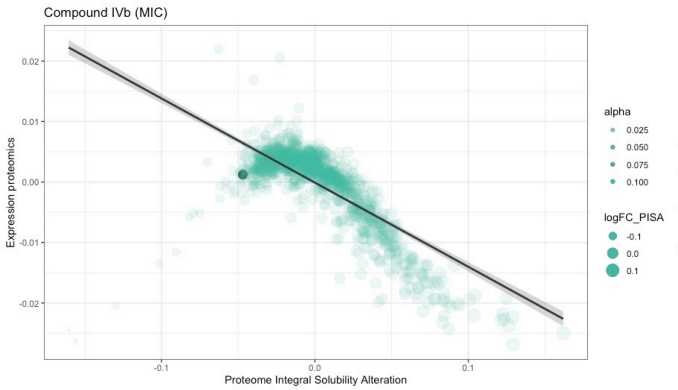
Compound IVb (MIC)
Expression proteomics
Proteome Integral Solubility Alteration
alpha
0.025
0.050
0.075
0.100
logFC_PISA
-0.1
0.0
0.1

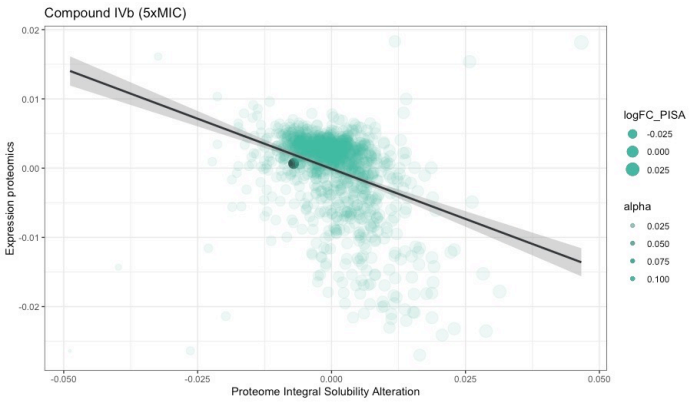
Compound IVb (5xMIC)
Expression proteomics
Proteome Integral Solubility Alteration
logFC_PISA
-0.025
0.000
0.025
alpha
0.025
0.050
0.075
0.100

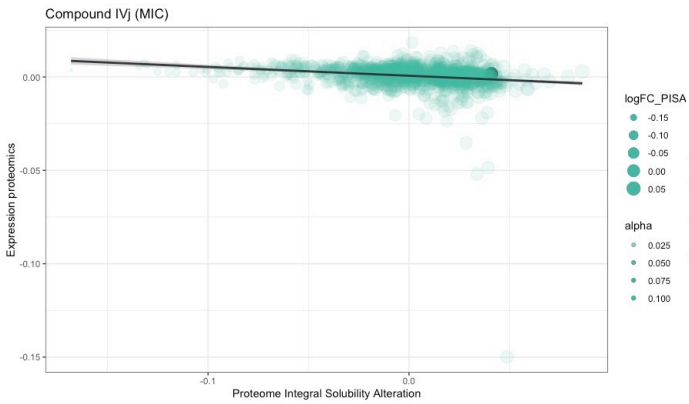
Compound IVj (MIC)
Expression proteomics
Proteome Integral Solubility Alteration
logFC_PISA
-0.15
-0.10
-0.05
0.00
0.05
alpha
0.025
0.050
0.075
0.100

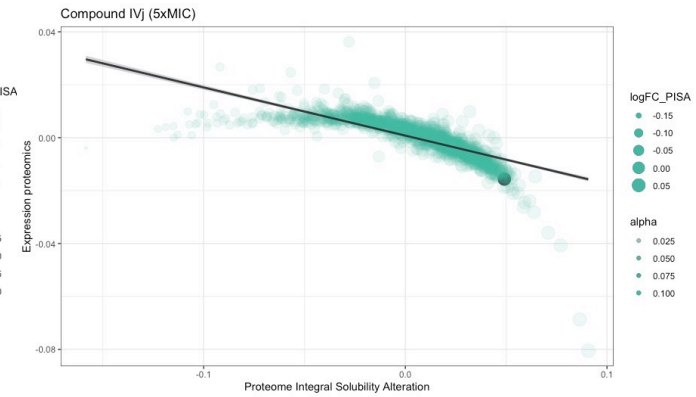
Compound IVj (5xMIC)
Expression proteomics
Proteome Integral Solubility Alteration
logFC_PISA
-0.15
-0.10
-0.05
0.00
0.05
alpha
0.025
0.050
0.075
0.100

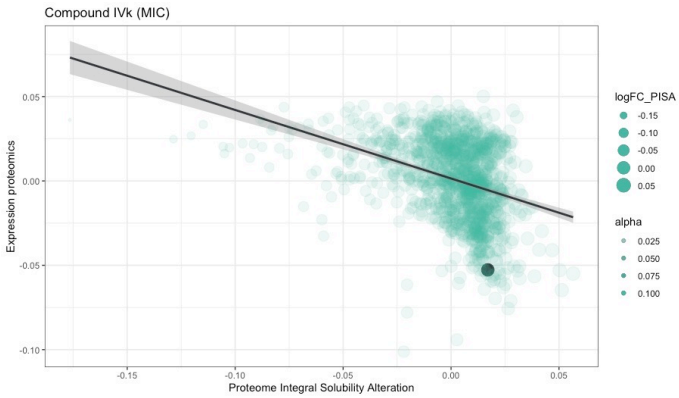
Compound IVk (MIC)
Expression proteomics
Proteome Integral Solubility Alteration
logFC_PISA
-0.15
-0.10
-0.05
0.00
0.05
alpha
0.025
0.050
0.075
0.100

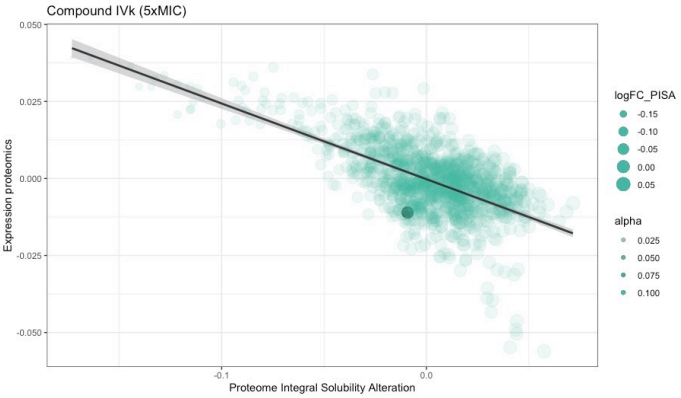
Compound IVk (5xMIC)
Expression proteomics
Proteome Integral Solubility Alteration
logFC_PISA
-0.15
-0.10
-0.05
0.00
0.05
alpha
0.025
0.050
0.075
0.100

Fig. S11 Alteration in solubility of flavodoxin in the Proteome Integral Solubility Alteration (PISA) assay associated with different compounds at two different concentrations. This figure provides information on the changes in solubility of flavodoxin under the influence of the tested compounds, highlighting potential differences in their effects on protein solubility.